

Computation of strongly coupled multifield interaction in particle–fluid systems

T.I. Zohdi *

Department of Mechanical Engineering, 6195 Etcheverry Hall, University of California, Berkeley, CA 94720-1740, USA

Received 1 November 2005; accepted 30 October 2006

Available online 24 March 2007

Abstract

The present work develops a flexible and robust solution strategy to resolve coupled systems comprised of large numbers of flowing particles embedded within a fluid. A model problem, consisting of particles which may undergo inelastic collisions in the presence of near-field forces, is considered. The particles are surrounded by a continuous interstitial fluid which is assumed to obey the compressible Navier–Stokes equations. Thermal effects are also considered. Such particle/fluid systems are strongly coupled, due to the mechanical forces and heat transfer induced by the fluid onto the particles and vice-versa. Because the coupling of the various particle and fluid fields can dramatically change over the course of a flow process, a primary focus of this work is the development of a recursive “staggering” solution scheme, whereby the time-steps are adaptively adjusted to control the error associated with the incomplete resolution of the coupled interaction between the various solid particulate and continuum fluid fields. A central feature of the approach is the ability to account for the presence of particles within the fluid in a straightforward manner that can be easily incorporated within any standard computational fluid mechanics code based on finite difference, finite element or finite volume type discretization. A three dimensional example is provided to illustrate the overall approach.

© 2007 Elsevier B.V. All rights reserved.

Keywords: Particle–fluid interaction; Multiple fields; Iterative methods

1. Introduction: multifield particle–fluid systems

A wide range of modern industrial and scientific applications has emerged where a successful analysis requires the simulation of flowing particulate media which incorporates near-field interaction between particles, interparticle contact and thermal effects, simultaneously.¹ For example, industrial processes such as Chemical Mechanical Planarization (CMP), which involves using chemically-reacting particles embedded within a fluid (gas or liquid) to ablate rough small-scale surfaces flat, have become important for the success of many micro- and nano-technologies, in particular for integrated circuit fabrication.² However, the process is still a technique of trial and error. During the last decade, understanding the basic mechanisms involved in this process has initiated research efforts in both industry and academia. For a review of CMP practice and applications, see Luo and Dornfeld [61–64]. It is clear that for the process to become viable and efficient,

* Tel.: +1 510 6429172; fax: +1 510 6425539.

¹ Here we use the term “near-field” interaction to denote the combination of attractive and repulsive forces.

² It is worth noting that, at the atomic scale, forces of attraction can arise from a temporary dipole created by fluctuating electron distributions around an atom. This will induce a dipole on a neighboring atom, and, if the induced dipole is directed in the same way as the first atom, two molecules associated with these atoms will attract one another. Between two atoms, such a force acts over a nanometer, however, when two small-scale (1–1000 μm) particles approach one another, the effect is greatly multiplied and the forces act over much larger distances. Furthermore, repulsion forces can arise due to ionization of the particle surfaces or due to the adsorption of ions onto the surfaces of particles.

the underlying physics must be modeled in a detailed, non-phenomenological, manner. The accurate simulation of CMP will require the description of the mechanics of fine-scale flowing particles, involving momentum exchange through mechanical contact between particles and thermo-chemical effects. Furthermore, because flowing particles below the one millimeter scale can acquire relatively large electrostatic charges, near-field effects must also be included. When dealing with fine-scale particles, the presence of near-field interaction forces can produce particulate flows that are radically different than purely contact-driven scenarios. For example, such near-field forces can lead to particle clustering, resulting in inconsistent planarization quality. Furthermore, neglecting such effects can lead to gross miscalculation of the power required to manipulate such flows. Thus, it is critical to develop models, and reliable techniques, to computationally simulate the dynamics of such multibody systems undergoing contact and near-field interaction simultaneously, within a fluid. Ultimately, the ability to perform rapid computational simulation of particle dynamics raises the possibility of *optimizing CMP-related parameters*, such as particle sizes, distributions, densities, grinding-pad surfaces, etc., for a given application.

In another realm, the natural sciences, the study of particle-laden dust clouds, stemming from ejecta (nickel, magnesium and iron) from comets and asteroids is becoming increasingly more important. A prominent example is the famous Tempel-Tuttle comet which passes through the solar system every 33 years. When the ejecta from this comet intersects the orbits of satellites, a number of difficulties can occur. Due to the increasingly rapid commercialization of near-earth space, and the presence of thousands of satellites, space-dust/satellite interaction problems are becoming of greater concern. Most larger objects, down to about the 0.1 m level, are tracked in low earth orbit. However, it is simply infeasible to track smaller sized dust.³ For example so-called “Leonids”, millimeter level clouds, so named because they appear to radiate from the head of the constellation of Leo the Lion, have been blamed for the malfunction of several man made satellites [10]. There are many more such debris clouds, such as Draconids, Lyrids, Perseids, Andromedids, etc., which are named for the constellations from which they appear to emanate. Such debris may not only lead to mechanical damage to the satellites, but can lead to instrumentation failure by disintegrating into charged particle-laden plasmas, which affect the sensitive electrical components on board. In another space-related area, dust clouds are also important in the formation of planetessimals, which are thought to initiate by the agglomeration of dust particles. For more information see Benz [12,13], Blum and Wurm [17], Dominik and Tielens [25], Chokshi et al. [20], Wurm et al. [92], Kokubu and Ida [49,50], Mitchell and Frenklach [66], Grazier et al. [39,40], Supulver and Lin [83], Tanga et al. [84], Cuzzi et al. [23], Weidenschilling and Cuzzi [88], Weidenschilling et al. [89], Beckwith et al. [11], Barge and Sommeria [6], Pollack et al. [69], Lissauer [59], Barranco et al. [7] and Barranco and Marcus [8,9].

Obviously, the number of research areas involving particles in a fluid undergoing various multifield processes is immense, and it would be futile to attempt to catalog all of the various applications. A common characteristic of such systems is that the various physical fields (thermal, mechanical, chemical, electrical, etc.) are strongly coupled. The goal of the present work is to develop a flexible and robust approach to solve such coupled systems. As a model problem we consider the interaction of large numbers of particles undergoing inelastic collisions and simultaneous interparticle (non-local) near-field attraction/repulsion. The particles are surrounded by a continuous interstitial fluid which is assumed to obey the compressible Navier–Stokes equations. The particle/fluid system is strongly coupled due to the drag-forces induced by the fluid onto the particles and vice-versa. In the modeling and simulations, thermal effects, such as radiative emission and convective heat transfer between the particles and the fluid, the generation of heat due to the drag-forces, thermal softening of the particles and the thermal dependency of the fluid viscosity, are included. Since the coupling of the various particle and fluid fields can dramatically change over the course of a flow process, the focus of this work is on the development of an iterative staggering solution scheme, whereby the time-steps are adaptively adjusted to control the error associated with the incomplete resolution of the coupled interaction between the various solid particulate and continuum fluid fields. The technique developed allows one to account for presence of particles in a manner which can easily be incorporated within any standard computational fluid mechanics code based on finite difference, finite element or finite volume type discretization.

2. A model problem

In order to present concepts thoroughly, we consider a sufficiently complex model problem comprised of a group of non-intersecting spherical particles (N_p in total).⁴ The equation of motion for the i th particle in the system is (Fig. 1)

$$m_i \ddot{\mathbf{r}}_i = \Psi_i^{\text{tot}}(\mathbf{r}_1, \mathbf{r}_2, \dots, \mathbf{r}_{N_p}), \quad (2.1)$$

where \mathbf{r}_i is the position vector of the i th particle and where Ψ_i^{tot} represents all forces acting on particle i . In particular, $\Psi_i^{\text{tot}} = \Psi_i^{\text{drag}} + \Psi_i^{\text{mf}} + \Psi_i^{\text{con}} + \Psi_i^{\text{fric}}$ represents the forces due to fluid drag, near-field interaction, interparticle contact forces

³ Ground-based radar, optical and infrared sensors routinely track several thousand objects daily.

⁴ It is assumed that the particles are small enough that the effects of their rotation with respect to their mass centers is unimportant (to the overall motion of the particle). However, even in the event that the particles are not extremely small, we assume that any “spin” of the particles is small enough to neglect lift forces that may arise from the interaction with the surrounding fluid.

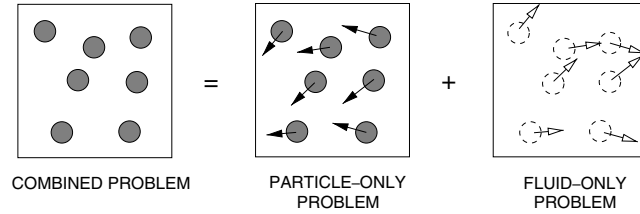


Fig. 1. Decomposition of the fluid/particle interaction.

and frictional forces. Clearly, under certain conditions one force may dominate over the others. However, this is generally impossible to ascertain a priori, since the dynamics and coupling in the system may change dramatically during the course of the flow process.

Remark: Throughout this work, boldface symbols indicate vectors or tensors. The inner product of two vectors \mathbf{u} and \mathbf{v} is denoted $\mathbf{u} \cdot \mathbf{v}$. At the risk of oversimplification, we ignore the distinction between second order tensors and matrices. Furthermore, we exclusively employ a Cartesian basis. Therefore, if we consider the second order tensor \mathbf{A} with its matrix representation $[\mathbf{A}]$, then the product of two second order tensors $\mathbf{A} \cdot \mathbf{B}$ is defined by the matrix product $[\mathbf{A}][\mathbf{B}]$. The second order inner product of two tensors or matrices is $\mathbf{A} : \mathbf{B} = \text{tr}([\mathbf{A}]^T[\mathbf{B}])$.

2.1. A simple characterization of particle/fluid interaction

We first consider drag-force interactions between the fluid and particles. The drag-force acting on an object in a fluid flow (occupying domain ω and outward surface normal \mathbf{n}) is defined as

$$\Psi^{\text{drag}} = \int_{\partial\omega} \boldsymbol{\sigma}_f \cdot \mathbf{n} dA, \tag{2.2}$$

where $\boldsymbol{\sigma}_f$ is the Cauchy-stress tensor. For a Newtonian fluid, $\boldsymbol{\sigma}_f$ is given by

$$\boldsymbol{\sigma}_f = -P_f \mathbf{1} + \lambda_f \text{tr} \mathbf{D}_f \mathbf{1} + 2\mu_f \mathbf{D}_f = -P_f \mathbf{1} + 3\kappa_f \frac{\text{tr} \mathbf{D}_f}{3} \mathbf{1} + 2\mu_f \mathbf{D}'_f, \tag{2.3}$$

where P_f is the thermodynamic pressure, $\kappa_f = \lambda_f + \frac{2}{3}\mu_f$ is the bulk viscosity, μ_f is the absolute viscosity, $\mathbf{D}_f = \frac{1}{2}(\nabla_x \mathbf{v}_f + (\nabla_x \mathbf{v}_f)^T)$ is the symmetric part of the velocity gradient, $\text{tr} \mathbf{D}_f$ is the trace of \mathbf{D}_f , and where $\mathbf{D}'_f = \mathbf{D}_f - \frac{\text{tr} \mathbf{D}_f}{3} \mathbf{1}$ is the deviatoric part of \mathbf{D}_f . The stress is determined by solving the following coupled system of partial differential equations (compressible Navier–Stokes):

Mass balance: $\frac{\partial \rho_f}{\partial t} = -\nabla_x \cdot (\rho_f \mathbf{v}_f)$ Energy balance: $\rho_f C_f \left(\frac{\partial \theta_f}{\partial t} + (\nabla_x \theta_f) \cdot \mathbf{v}_f \right) = \boldsymbol{\sigma}_f : \nabla_x \mathbf{v}_f + \nabla_x \cdot (\mathbb{K}_f \cdot \nabla \theta_f) + \rho_f z_f,$ Momentum balance: $\rho_f \left(\frac{\partial \mathbf{v}_f}{\partial t} + (\nabla_x \mathbf{v}_f) \cdot \mathbf{v}_f \right) = \nabla_x \cdot \boldsymbol{\sigma}_f + \rho_f \mathbf{b}_f,$	(2.4)
--	-------

where, at a point, ρ_f is the fluid density, \mathbf{v}_f is the fluid velocity, θ_f is the fluid temperature, C_f is the fluid heat capacity, z_f is the heat source per unit mass, \mathbb{K}_f is the thermal conductivity tensor, assumed to be isotropic of the form $\mathbb{K}_f = K_f \mathbf{1}$, K_f being the scalar thermal conductivity and where \mathbf{b}_f represents body forces per unit mass. The thermodynamic pressure is given by an equation of state,

$$\mathcal{L}(P_f, \rho_f, \theta_f) = 0. \tag{2.5}$$

The specific form of the equation of state will be discussed later in the presentation.

The fluid domain will require spatial discretization with some type of mesh, in conjunction with, for example, a finite difference, finite volume or finite element method. Usually, it is extremely difficult to resolve the flow in the immediate neighborhood of the particles, in particular if there are several particles. However, if the primary interest is in the dynamics of the particles, *as it is in this work*, an appropriate approach, which permits a coarser discretization of the fluid continuum, is to employ effective drag coefficients, for example, defined via

$$C_D \stackrel{\text{def}}{=} \frac{\|\Psi_i^{\text{drag}}\|}{\frac{1}{2} \langle \rho_f \rangle_{\omega_i} \|\langle \mathbf{v}_f \rangle_{\omega_i} - \mathbf{v}_i\|^2 A_i}, \tag{2.6}$$

where $\langle (\cdot) \rangle_{\omega_i} \stackrel{\text{def}}{=} \frac{1}{|\omega_i|} \int_{\omega_i} (\cdot) d\omega_i$ is the volumetric average of the argument over the domain occupied by the i th particle, $\langle \mathbf{v}_f \rangle_{\omega_i}$ is the volumetric average of the fluid velocity, \mathbf{v}_i is the velocity of the i th (solid) particle and where A_i is the

cross-sectional area of the i th (solid) particle. For example, one possible way to represent the drag coefficient is with a piecewise definition, as a function of the Reynolds number [21]:

- for $0 < Re \leq 1$, $C_D = \frac{24}{Re}$,
- for $1 < Re \leq 400$, $C_D = \frac{24}{Re^{0.646}}$,
- for $400 < Re \leq 3 \times 10^5$, $C_D = 0.5$,
- for $3 \times 10^5 < Re \leq 2 \times 10^6$, $C_D = 0.000366Re^{0.4275}$,
- for $2 \times 10^6 < Re < \infty$, $C_D = 0.18$,

where the local Reynolds number for a particle is $Re \stackrel{\text{def}}{=} \frac{2b_i \langle \rho_f \rangle_{\omega_i} \| \langle \mathbf{v}_f \rangle_{\omega_i} - \mathbf{v}_i \|}{\mu}$ and where b_i is the radius of the i th particle. The use of this simple concept is relatively straightforward to account for the presence of the solid particles in the fluid by augmenting the flow calculations with drag-forces (Fig. 1). Algorithmically speaking, one must compute the fluid flow with reaction forces due to the presence of the particles. To this end, one can use the volumetric forces (\mathbf{b}_f) and heat sources (z_f) within the fluid domain for this purpose by writing

$$\begin{aligned} \rho_f \left(\frac{\partial \mathbf{v}_f}{\partial t} + (\nabla_x \mathbf{v}_f) \cdot \mathbf{v}_f \right) &= \nabla_x \cdot \boldsymbol{\sigma}_f + \rho_f \mathbf{b}_f, \\ \mathbf{b}_f &= \mathbf{b}_D = - \frac{\boldsymbol{\Psi}_i^{\text{drag}}}{m_i} = - \frac{C_D \frac{1}{2} \langle \rho_f \rangle_{\omega_i} \| \langle \mathbf{v}_f \rangle_{\omega_i} - \mathbf{v}_i \|^2 A_i}{m_i} \mathbf{d}, \quad \left(\mathbf{d} = \frac{\langle \mathbf{v}_f \rangle_{\omega_i} - \mathbf{v}_i}{\| \langle \mathbf{v}_f \rangle_{\omega_i} - \mathbf{v}_i \|} \right), \\ \rho_f C \left(\frac{\partial \theta_f}{\partial t} + (\nabla_x \theta_f) \cdot \mathbf{v}_f \right) &= \boldsymbol{\sigma}_f : \nabla_x \mathbf{v}_f + \nabla_x \cdot (\mathbb{K}_f \cdot \nabla_x \theta_f) + \rho_f z_f, \\ z_f &= z_D = c_v |\mathbf{b}_D \cdot (\langle \mathbf{v}_f \rangle_{\omega_i} - \mathbf{v}_i)|, \end{aligned} \quad (2.7)$$

where the drag-force on the fluid \mathbf{b}_D (per unit mass), is non-zero if its location coincides with the particle domain, and is zero otherwise. Here, z_D is the heat source due to the rate of work done by the drag-force on the fluid.⁵ Such source terms are easily projected onto a finite difference or finite element grid.⁶ *This drag-based approach is designed to account for particles in the fluid using a coarse mesh. In other words, the smallest (mesh) scale allowable is that associated with the dimensions of the particles. Accordingly, we shall not employ meshes smaller than the particle length scale when simulations are performed later.*

Remarks: More detailed analyses of fluid–particle interaction can be achieved in two primary ways: (1) direct, brute-force, numerical schemes, treating the particles as part of the fluid continuum (as another fluid or solid phase), and thus meshing them in a detailed manner, or (2) with semi-analytical techniques, for example such as those based on approximation of the interaction between the particles and the fluid, employing an analysis of the (interstitial) fluid gaps using lubrication theory. For a concise review of recent developments in such semi-analytical techniques, in particular methods which go beyond local analyses of flow in a single fluid gap, using discrete network approximations, which account for multiple hydrodynamic interactions, see Berlyand and Panchenko [15,16]. Although not employed here, discrete network approximations appear to be quite attractive for possibly improving the description of the interaction between the particles and the fluid, beyond a simple drag-based method, as adopted in this work, without resorting to detailed numerical meshing.

2.2. Particle thermodynamics

Throughout the thermal analysis of the particles, we shall use relatively simple models. Consistent with the particle-based philosophy, it is assumed that the temperature within each particle is uniform (a lumped mass approximation). We remark that the validity of assuming a uniform temperature within a particle is dictated by the Biot number. A small Biot number indicates that such an approximation is reasonable. The Biot number, for a sphere, scales with the ratio of particle volume (V) to particle surface area (a_s), $\frac{V}{a_s} = \frac{b}{3}$, which indicates that a uniform temperature distribution is appropriate, since the particles are, by definition, small. Since it is assumed that the temperature fields are uniform within the particles, the gradient of the temperature within the particle is zero, i.e. $\nabla \theta = \mathbf{0}$. Therefore, a Fourier-type law for the heat flux will register a zero value, $\mathbf{q} = -\mathbb{K} \cdot \nabla \theta = \mathbf{0}$.

Under these assumptions, we consider an energy balance, governing the interconversions of mechanical, thermal and chemical energy in a system, dictated by the First Law of Thermodynamics. Accordingly, we require the time rate of

⁵ If the constant c_v is not selected as unity, this can indicate endothermic or exothermic particle/fluid chemical reactions.

⁶ If the particles are significantly smaller than the mesh spacing, then the drag-forces associated with the particles are computed from the nearest node/particle center pair.

change of the sum of the kinetic energy (\mathcal{K}) and stored energy (\mathcal{S}) to be equal to the work rate (power, \mathcal{P}) and the net heat supplied (\mathcal{H})

$$\frac{d}{dt}(\mathcal{K} + \mathcal{S}) = \mathcal{P} + \mathcal{H}, \tag{2.8}$$

where we assume that the stored energy is comprised solely of a thermal part, $\mathcal{S} = mC\theta$, C being the heat capacity per unit mass. Consistent with an assumption that the particles deform negligibly during impact, *the amount of stored mechanical energy is deemed insignificant*. The kinetic energy is $\mathcal{K} = \frac{1}{2}m\mathbf{v} \cdot \mathbf{v}$. The mechanical power term is due to the forces acting on a particle

$$\mathcal{P} = \frac{d\mathcal{W}}{dt} = \boldsymbol{\Psi}^{\text{tot}} \cdot \mathbf{v}. \tag{2.9}$$

For the particles, it is assumed that a process of convection, for example governed by Newton’s law of cooling and thermal radiation according to a simple Stefan–Boltzmann law, transpires. Accordingly, the First Law reads

$$\underbrace{m\dot{\mathbf{v}} \cdot \mathbf{v} + mC\dot{\theta}}_{\frac{d(\mathcal{K}+\mathcal{S})}{dt}} = \underbrace{\boldsymbol{\Psi}^{\text{tot}} \cdot \mathbf{v}}_{\text{power}=\mathcal{P}} - \underbrace{\underbrace{h_c a_s (\theta - \theta_0)}_{\text{convection}} + \underbrace{m c_v |\mathbf{b}_D \cdot (\langle \mathbf{v}_f \rangle_\omega - \mathbf{v})|}_{\text{drag}} - \underbrace{\mathcal{B} a_s \epsilon (\theta^4 - \theta_s^4)}_{\text{radiation}}}_{\mathcal{H}}, \tag{2.10}$$

where θ_0 is the local temperature of the ambient fluid, h_c is the convection coefficient (using Newton’s Law of cooling) and where θ_s is the temperature of the far field surface (for example a container surrounding the flow) with which radiative exchange is made. The Stefan–Boltzmann constant is $\mathcal{B} = 5.67 \times 10^{-8} \frac{\text{W}}{\text{m}^2 \text{K}}$, $0 \leq \epsilon \leq 1$ is the emissivity, which indicates how efficiently the surface radiates energy compared to a black-body (an ideal emitter), and a_s is the surface area of a particle. It is assumed that the radiation exchange between the particles is negligible.⁷ We recall that a blackbody is an ideal radiating surface having the following properties: (1) It absorbs all incident radiation, regardless of wavelength and direction, (2) For a prescribed temperature and wavelength, no surface can emit more energy than a blackbody and (3) Although the radiation emitted by a blackbody is a function of wavelength and temperature, it is independent of direction. Since a blackbody is a perfect emitter, it serves as a baseline against which the radiative properties of actual surfaces may be compared. The Stefan–Boltzmann law, which is computed by integrating the Planck representation of the emissive power distribution of a blackbody over all wavelengths, allows the calculation of the amount of radiation emitted in all directions and over all wavelengths simply from the knowledge of the temperature of the blackbody. Because $\frac{d\mathcal{K}}{dt} = m\dot{\mathbf{v}} \cdot \mathbf{v} = \boldsymbol{\Psi}^{\text{tot}} \cdot \mathbf{v} = \mathcal{P}$, we obtain a simplified form of the First Law, $\frac{d\mathcal{S}}{dt} = \mathcal{H}$, and therefore Eq. (2.10) becomes

$$mC\dot{\theta} = -h_c a_s (\theta - \theta_0) + m c_v |\mathbf{b}_D \cdot (\langle \mathbf{v}_f \rangle_\omega - \mathbf{v})| - \mathcal{B} a_s \epsilon (\theta^4 - \theta_s^4), \tag{2.11}$$

where $\theta_0 = \langle \theta_f \rangle_\omega$ is the local average of the surrounding fluid temperature.

Remarks: To account for the convective exchange between the fluid and particles, we amend the source term in Eq. (2.7) for the fluid to read

$$z_f = z_D = c_v |\mathbf{b}_f \cdot (\langle \mathbf{v}_f \rangle_\omega - \mathbf{v})| + \frac{h_c a_s (\theta - \theta_0)}{m}. \tag{2.12}$$

If the fluid is “radiationally thick”, then we assume that no radiation enters the system from the far field, namely that $\mathcal{B} a_s \epsilon \theta_s^4 = 0$ in Eq. (2.11), and that any emission from the particle gets absorbed by the fluid. Thus, in that situation, we can again amend the source term to read

$$z_f = z_D = c_v |\mathbf{b}_f \cdot (\langle \mathbf{v}_f \rangle_\omega - \mathbf{v})| + \frac{h_c a_s (\theta - \theta_0) + \mathcal{B} a_s \epsilon \theta^4}{m}. \tag{2.13}$$

2.3. A model for near-field interaction and particle contact

Following the approach found in Zohdi [96–98] for dry (fluid-free) particulate flows, we consider the following, relatively general, central-force attraction-repulsion form for the near-field forces (in Eq. (2.1)) induced by all particles on particle i

⁷ Various arguments for such an assumption can be found in the classical text of Bohren and Huffman [18].

$$\Psi_i^{\text{nf}} = \sum_{j \neq i}^{N_p} \left(\left(\underbrace{\alpha_1 \|\mathbf{r}_i - \mathbf{r}_j\|^{-\beta_1}}_{\text{attractive part}} - \underbrace{\alpha_2 \|\mathbf{r}_i - \mathbf{r}_j\|^{-\beta_2}}_{\text{repulsive part}} \right) \underbrace{\mathbf{n}_{ij}}_{\text{unit vector}} \right), \quad (2.14)$$

where $\|\cdot\|$ represents the Euclidean norm (distance) in R^3 , where all of the parameters, α 's and β 's, are non-negative, and where the normal direction is determined by the difference in the position vectors of their centers, $\mathbf{n}_{ij} \stackrel{\text{def}}{=} \frac{\mathbf{r}_j - \mathbf{r}_i}{\|\mathbf{r}_j - \mathbf{r}_i\|}$. Provided that the exponents are suitably chosen in Eq. (2.14), namely $\frac{\beta_2}{\beta_1} > 1$, the force interaction of the form chosen is stable, in the sense that for small disturbances, the system will remain near an equilibrium position, as opposed to unstable equilibrium, where perturbations cause the system to move away from an equilibrium position, with an increasing velocity. We refer the reader to Appendix A for details. More complex interaction force-forms modeling, for example, binding forces can be found in Zohdi [98]. There are similarities between particulate flow models and those found in the field of Molecular Dynamics (MD), where the motion of individual atoms is described by the Newton's Second Law with the forces computed from a prescribed potential energy function, $V(\mathbf{r})$, $m\ddot{\mathbf{r}} = -\nabla V(\mathbf{r})$. For reviews of MD, see Haile [41], Hase [43], Schlick [76] or Rapaport [74]. More complex (tertiary and binary) potentials are possible, and take the form of familiar Mie, Lennard-Jones, and Morse potentials [67]. The expansions beyond the binary interactions introduce either three-body terms directly [80] or as modifications of the two-body representations [86]. For reviews, we refer the reader to Frenklach and Carmer [36]. Depending on the degree of near-field strength, the particulate system can exhibit vibratory motion. This can be qualitatively explained by recognizing that the governing equations are formally similar to classical second order equations describing harmonic oscillators. For more details, see Zohdi [96,98].

2.3.1. Normal contact

We now consider particle contact in the presence of near-field forces. We assume that the particles remain spherical after impact, i.e. any permanent deformation is negligible. Also, in contrast with the usual analyses of impacting particles, which neglect all other forces except those of mechanical contact, we include the near-field effects and other external forces, for example due to fluid drag. For two impacting particles i and j , normal to the line of impact, a statement for a balance of linear momentum relating the states before impact (time = t) and after impact (time = $t + \delta t$) reads as

$$m_i v_{in}(t) + m_j v_{jn}(t) + \int_t^{t+\delta t} \mathbf{E}_i \cdot \mathbf{n}_{ij} dt + \int_t^{t+\delta t} \mathbf{E}_j \cdot \mathbf{n}_{ij} dt = m_i v_{in}(t + \delta t) + m_j v_{jn}(t + \delta t), \quad (2.15)$$

where the subscript n denotes the normal component of the velocity (along the line connecting particle centers) and the \mathbf{E} 's represent all forces induced by near-field interaction with other particles, as well as all other external forces, if any (for example drag), to the pair. If one isolates one of the members of the colliding pair, then

$$m_i v_{in}(t) + \int_t^{t+\delta t} I_n dt + \int_t^{t+\delta t} \mathbf{E}_i \cdot \mathbf{n}_{ij} dt = m_i v_{in}(t + \delta t), \quad (2.16)$$

where $\int_t^{t+\delta t} I_n dt$ is the total normal impulse due to impact. For a pair of particles undergoing impact, let us consider a decomposition of the collision event into a compression (δt_1) and recovery (δt_2) phase, i.e. $\delta t = \delta t_1 + \delta t_2$. Between the compression and recovery phases, the particles achieve a common velocity, denoted v_{cn} , at the intermediate time $t + \delta t_1$. A common normal velocity for particles should be interpreted as indicating that the relative velocity in the normal direction between particle centers is zero. We may write for particle i , along the normal, in the compression phase of impact

$$m_i v_{in}(t) + \int_t^{t+\delta t_1} I_n dt + \int_t^{t+\delta t_1} \mathbf{E}_i \cdot \mathbf{n}_{ij} dt = m_i v_{cn} \quad (2.17)$$

and in the recovery phase

$$m_i v_{cn} + \int_{t+\delta t_1}^{t+\delta t} I_n dt + \int_{t+\delta t_1}^{t+\delta t} \mathbf{E}_i \cdot \mathbf{n}_{ij} dt = m_i v_{in}(t + \delta t). \quad (2.18)$$

For the other particle (j), in the compression phase,

$$m_j v_{jn}(t) - \int_t^{t+\delta t_1} I_n dt + \int_t^{t+\delta t_1} \mathbf{E}_j \cdot \mathbf{n}_{ij} dt = m_j v_{cn} \quad (2.19)$$

and in the recovery phase

$$m_j v_{cn} - \int_{t+\delta t_1}^{t+\delta t} I_n dt + \int_{t+\delta t_1}^{t+\delta t} \mathbf{E}_j \cdot \mathbf{n}_{ij} dt = m_j v_{jn}(t + \delta t). \quad (2.20)$$

This leads to an expression for the coefficient of restitution

$$e \stackrel{\text{def}}{=} \frac{\int_t^{t+\delta t} I_n dt}{\int_t^{t+\delta t_1} I_n dt} = \frac{m_i(v_{in}(t + \delta t) - v_{cn}) - E_{in}(t + \delta t_1, t + \delta t)}{m_i(v_{cn} - v_{in}(t)) - E_{in}(t, t + \delta t_1)} = \frac{-m_j(v_{jn}(t + \delta t) - v_{cn}) + E_{jn}(t + \delta t_1, t + \delta t)}{-m_j(v_{cn} - v_{jn}(t)) + E_{jn}(t, t + \delta t_1)}, \quad (2.21)$$

where

$$E_{in}(t + \delta t_1, t + \delta t_2) \stackrel{\text{def}}{=} \int_{t+\delta t_1}^{t+\delta t} \mathbf{E}_i \cdot \mathbf{n}_{ij} dt, \quad E_{jn}(t + \delta t_1, t + \delta t_2) \stackrel{\text{def}}{=} \int_{t+\delta t_1}^{t+\delta t} \mathbf{E}_j \cdot \mathbf{n}_{ij} dt, \\ E_{in}(t, t + \delta t_1) \stackrel{\text{def}}{=} \int_t^{t+\delta t_1} \mathbf{E}_i \cdot \mathbf{n}_{ij} dt, \quad E_{jn}(t, t + \delta t_1) \stackrel{\text{def}}{=} \int_t^{t+\delta t_1} \mathbf{E}_j \cdot \mathbf{n}_{ij} dt. \quad (2.22)$$

If we eliminate v_{cn} , we obtain an expression for e

$$e = \frac{v_{jn}(t+\delta t) - v_{in}(t+\delta t) + D_{ij}(t+\delta t_1, t+\delta t)}{v_{in}(t) - v_{jn}(t) + D_{ij}(t, t+\delta t_1)}, \quad (2.23)$$

where we define the operator over any time interval (a, b) as $D_{ij}(a, b) \stackrel{\text{def}}{=} \frac{1}{m_i} E_{in}(a, b) - \frac{1}{m_j} E_{jn}(a, b)$. Thus, we may rewrite Eq. (2.23) as

$$v_{jn}(t + \delta t) = v_{in}(t + \delta t) - D_{ij}(t + \delta t_1, t + \delta t) + e(v_{in}(t) - v_{jn}(t) + D_{ij}(t, t + \delta t_1)). \quad (2.24)$$

It is convenient to denote the average force acting on the particle from external sources as $\bar{E}_{im} \stackrel{\text{def}}{=} \frac{1}{\delta t} \int_t^{t+\delta t} \mathbf{E}_i \cdot \mathbf{n}_{ij} dt$. If e is explicitly known, then one can write, combining Eqs. (2.23) and (2.15)

$$v_{in}(t + \delta t) = \frac{m_i v_{in}(t) + m_j(v_{jn}(t) - e(v_{in}(t) - v_{jn}(t)))}{m_i + m_j} + \frac{(\bar{E}_{im} + \bar{E}_{jm})\delta t - m_j(eD_{ij}(t, t + \delta t_1) - D_{ij}(t + \delta t_1, t + \delta t))}{m_i + m_j}, \quad (2.25)$$

where, once $v_{in}(t + \delta t)$ is known, one can subsequently also solve for $v_{jn}(t + \delta t)$ via Eq. (2.24).

Remark 1. Clearly, the forces needed to compute terms in coefficient of restitution e , such as E_{im} , E_{jm} and D_{ij} depend on the particle kinetics during impact, i.e. the outcome of the system dynamics, and thus implicitly on e . In other words, an implicit system of nonlinear coupled equations arises. In order to solve the system of coupled nonlinear equations, later in this work, an iterative (fixed-point type) staggering process is developed.

Remark 2. Eq. (2.23) collapses to the classical expression for the ratio of the relative velocities before and after impact, if the near-field forces are negligible,

$$e \stackrel{\text{def}}{=} \frac{v_{jn}(t + \delta t) - v_{in}(t + \delta t)}{v_{in}(t) - v_{jn}(t)}. \quad (2.26)$$

Later, it will be useful to define the average impulsive normal contact force between the particles acting during the impact event as

$$\bar{I}_n \stackrel{\text{def}}{=} \frac{1}{\delta t} \int_t^{t+\delta t} I_n dt = \frac{m_i(v_{in}(t + \delta t) - v_{in}(t))}{\delta t} - \bar{E}_{in}. \quad (2.27)$$

In particular, as will be done later in the analysis, when we discretize the equations of motion with a discrete (finite difference) time-step of Δt , where $\delta t \ll \Delta t$, we shall define the impulsive normal contact contribution to the total force (Eq. (2.1)) to be

$$\Psi^{\text{con}} = \frac{\bar{I}_n \delta t}{\Delta t} \mathbf{n}_{ij}, \quad (2.28)$$

which will be included in the total force acting on a particle, $\Psi_i^{\text{tot}} = \Psi_i^{\text{drag}} + \Psi_i^{\text{nf}} + \Psi_i^{\text{con}} + \Psi_i^{\text{fric}}$. Furthermore, at the implementation level, we choose $\delta t = \gamma \Delta t$, where $0 < \gamma \ll 1$ and where Δt is the time-step discretization size, which will be introduced later in the work.⁸ We assume $\delta t_1 + \delta t_2 = \delta t_1 + e\delta t_1$, which immediately allows the following definitions

$$\delta t_1 = \frac{\gamma \Delta t}{1 + e} \quad \text{and} \quad \delta t_2 = \frac{e\gamma \Delta t}{1 + e}. \quad (2.29)$$

These results are consistent with the fact that the recovery time vanishes (all compression and no recovery) for $e \rightarrow 0$ (asymptotically plastic) and, as $e \rightarrow 1$, the recovery time equals the compression time ($\delta t_2 = \delta t_1$, asymptotically elastic). For a more detailed treatment of impact duration times, see Johnson [44].

⁸ A typical choice is $0 < \gamma \leq 0.01$. The system is insensitive to γ below 0.01.

2.3.2. Friction

To account for frictional stick-slip phenomena, during impact for an arbitrary particle pair (i and j), the tangential velocities at the beginning of the impact time interval, time = t , are computed by subtracting the relative normal velocity away from the total relative velocity,

$$\mathbf{v}_{jt}(t) - \mathbf{v}_{it}(t) = (\mathbf{v}_j(t) - \mathbf{v}_i(t)) - ((\mathbf{v}_j(t) - \mathbf{v}_i(t)) \cdot \mathbf{n}_{ij})\mathbf{n}_{ij}. \quad (2.30)$$

One then writes the equation for tangential momentum change during impact for the i th particle $m_i v_{it}(t) - \bar{I}_f \delta t + \bar{E}_{it} \delta t = m_i v_{ct}$, where the friction contribution is $\bar{I}_f = \frac{1}{\delta t} \int_t^{t+\delta t} I_f dt$, where the total contributions from all other particles in the tangential direction (\mathbf{t}_{ij}) are $\bar{E}_{it} = \frac{1}{\delta t} \int_t^{t+\delta t} \mathbf{E}_i \cdot \mathbf{t}_{ij} dt$ and where v_{ct} is the common tangential velocity of particles i and j in the tangential direction.⁹ Similarly, for the j th particle we have $m_j v_{jt}(t) + \bar{I}_f \delta t + \bar{E}_{jt} \delta t = m_j v_{ct}$. There are two unknowns, \bar{I}_f and v_{ct} . The main quantity of interest is \bar{I}_f , which can be solved for

$$\bar{I}_f = \frac{(m_j \bar{E}_{it} - m_i \bar{E}_{jt}) \delta t + m_i m_j (v_{it}(t) - v_{jt}(t))}{(m_i + m_j) \delta t}. \quad (2.31)$$

The friction force is then $\Psi_i^{\text{fric}} = |\bar{I}_f| \mathbf{t}_{ij}$. However, consistent with stick-slip models of Coloumb friction, one first assumes no slip occurs. If $|\bar{I}_f| > \mu_s |\bar{I}_n|$, where μ_s is the coefficient of *static* friction, then slip must occur and a dynamic sliding friction model is used. If sliding occurs, the friction force is assumed to be proportional to the normal force and opposite to the direction of relative tangent motion, i.e.

$$\Psi_i^{\text{fric}} \stackrel{\text{def}}{=} \mu_d \|\Psi^{\text{con}}\| \frac{\mathbf{v}_{jt} - \mathbf{v}_{it}}{\|\mathbf{v}_{jt} - \mathbf{v}_{it}\|} = -\Psi_j^{\text{fric}}, \quad (2.32)$$

where μ_d the dynamic coefficient of friction and where $\mu_d \leq \mu_s$. There are limitations on the friction coefficients for such models to make physical sense. For general dynamic analyses of such mechanical models involving friction see Oden and Pires [68], Martins and Oden [65], Kikuchi and Oden [47], Klarbring [48] or Cho and Barber [19]. For a recent overview, see Wrighgers [91].

2.3.3. Contact-thermal sensitivity

It is important to realize that, in reality, the phenomenological parameter e depends on the severity of the impact velocity. For extensive experimental data, see Goldsmith [38]. Qualitatively, the coefficient of restitution will decrease with the relative velocity of approach. A mathematical idealization of the behavior can be constructed as follows:

$$e \stackrel{\text{def}}{=} \max \left(e_0 \left(1 - \frac{\Delta v_n}{v^*} \right), e^- \right), \quad (2.33)$$

where v^* is a critical threshold velocity (normalization) parameter and where the relative velocity of approach is defined by $\Delta v_n \stackrel{\text{def}}{=} |v_{jn}(t) - v_{in}(t)|$ and e^- is a (typically small) lower limit to the coefficient of restitution.¹⁰

In many cases, thermal effects during the impact process are important. For instance, the presence of a reactive substance (gas) adsorbed onto the surface of interplanetary dust can be a source of intense heat generation, through thermochemical reactions activated by impact forces, which thermally soften the material, thus reducing the coefficient of restitution, which in turn strongly affects the mechanical impact event itself.¹¹ Also, in the previously mentioned industrial CMP processes, induced (deliberate) particle reactivity is commonplace. A somewhat ad-hoc approach, building on the relation in Eq. (2.33), is to construct a thermally dependent coefficient of restitution as follows [98]:

$$e \stackrel{\text{def}}{=} \left(\max \left(e_0 \left(1 - \frac{\Delta v_n}{v^*} \right), e^- \right) \right) \left(\max \left(\left(1 - \frac{\theta}{\theta^*} \right), 0 \right) \right), \quad (2.34)$$

where θ^* can be considered as a thermal softening temperature.¹²

3. Numerical discretization of the Navier–Stokes equations

We now develop a fully implicit staggering scheme, in conjunction with a finite difference discretization, to solve the coupled system. Generally, such schemes proceed, within a discretized time-step, by solving each field equation individually, allowing only the corresponding primary field variable (ρ_f , \mathbf{v}_f or θ_f) to be active. This effectively (momentarily) decou-

⁹ They do not move relative to one another.

¹⁰ Lower values of v^* represent softer materials, which exhibit more dissipation upon impact than harder materials.

¹¹ This is discussed shortly.

¹² Lower values of θ^* represent more thermally sensitive materials, with relatively more dissipative impact events. Generally, decreasing v^* and θ^* makes the system more dissipative and, consequently, easier to simulate, since it is less stiff.

ples the system of differential equations. After the solution of each field equation, the primary field variable is updated, and the next field equation is solved in a similar manner, with only the corresponding primary variable being active. For accurate numerical solutions, the approach requires small time-steps, primarily because the staggering error accumulates with each passing increment. Thus, such computations are usually computationally intensive.

First, let us consider a finite difference discretization of the derivatives in the governing equations where, for brevity, we write (L indicates the time-step counter, $\mathbf{v}_f^L \stackrel{\text{def}}{=} \mathbf{v}_f(t)$, $\mathbf{v}_f^{L+1} \stackrel{\text{def}}{=} \mathbf{v}_f(t + \Delta t)$, etc.) for each finite difference node (i, j, k)

$$\begin{aligned}
 \rho_f^{i,j,k,L+1} &= \rho_f^{i,j,k,L} - \Delta t (\nabla_x \cdot (\rho_f \mathbf{v}_f))^{i,j,k,L+1}, \\
 \mathcal{L}(P_f^{i,j,k,L+1}, \rho_f^{i,j,k,L+1}, \theta_f^{i,j,k,L+1}) &= 0, \\
 \theta_f^{i,j,k,L+1} &= \theta_f^{i,j,k,L} - \Delta t (\nabla_x \theta_f \cdot \mathbf{v}_f)^{i,j,k,L+1} + \left(\frac{\Delta t}{\rho_f C_f} (\boldsymbol{\sigma}_f : \nabla_x \mathbf{v}_f + \nabla_x \cdot (\mathbb{K}_f \cdot \nabla_x \theta_f) + \rho_f z_f) \right)^{i,j,k,L+1}, \\
 \mathbf{v}_f^{i,j,k,L+1} &= \mathbf{v}_f^{i,j,k,L} - \Delta t (\nabla_x \mathbf{v}_f \cdot \mathbf{v}_f)^{i,j,k,L+1} + \frac{\Delta t}{\rho_f} (\nabla_x \cdot \boldsymbol{\sigma}_f + \rho_f \mathbf{b}_f)^{i,j,k,L+1},
 \end{aligned} \tag{3.1}$$

where the derivatives are computed by the following; for the continuity equation:

$$\begin{aligned}
 \left(\frac{\partial \rho_f}{\partial t} \right)^{i,j,k,L} &\approx \frac{\rho_f(x_1, x_2, x_3, t + \Delta t) - \rho_f(x_1, x_2, x_3, t)}{\Delta t} = \frac{\rho_f^{i,j,k,L+1} - \rho_f^{i,j,k,L}}{\Delta t}, \\
 \nabla_x \cdot (\rho_f \mathbf{v}_f) &\approx \frac{(\rho_f v_{f1})^{i+1,j,k,L} - (\rho_f v_{f1})^{i-1,j,k,L}}{2\Delta x_1} \\
 &\quad + \frac{(\rho_f v_{f2})^{i,j+1,k,L} - (\rho_f v_{f2})^{i,j-1,k,L}}{2\Delta x_2} \\
 &\quad + \frac{(\rho_f v_{f3})^{i,j,k+1,L} - (\rho_f v_{f3})^{i,j,k-1,L}}{2\Delta x_3}
 \end{aligned} \tag{3.2}$$

for the balance of energy

$$\begin{aligned}
 \left(\rho_f C_f \frac{\partial \theta_f}{\partial t} \right)^{i,j,k,L} &\approx \rho_f^{i,j,k,L} C_f \frac{(\theta_f^{i,j,k,L+1} - \theta_f^{i,j,k,L})}{\Delta t}, \\
 \left(\rho_f C_f \nabla_x \theta_f \cdot \mathbf{v}_f \right)^{i,j,k,L} &\approx \rho_f^{i,j,k,L} C_f \left(v_{f1}^{i,j,k,L} \frac{\theta_f^{i+1,j,k,L} - \theta_f^{i-1,j,k,L}}{2\Delta x_1} + v_{f2}^{i,j,k,L} \frac{\theta_f^{i,j+1,k,L} - \theta_f^{i,j-1,k,L}}{2\Delta x_2} + v_{f3}^{i,j,k,L} \frac{\theta_f^{i,j,k+1,L} - \theta_f^{i,j,k-1,L}}{2\Delta x_3} \right), \\
 \left(\boldsymbol{\sigma}_f : \nabla_x \mathbf{v}_f \right)^{i,j,k,L} &\approx \sigma_{f11}^{i,j,k,L} \frac{v_{f1}^{i+1,j,k,L} - v_{f1}^{i-1,j,k,L}}{2\Delta x_1} + \sigma_{f22}^{i,j,k,L} \frac{v_{f2}^{i,j+1,k,L} - v_{f2}^{i,j-1,k,L}}{2\Delta x_2} + \sigma_{f33}^{i,j,k,L} \frac{v_{f3}^{i,j,k+1,L} - v_{f3}^{i,j,k-1,L}}{2\Delta x_3} \\
 &\quad + \sigma_{f12}^{i,j,k,L} \left(\frac{v_{f1}^{i+1,j,k,L} - v_{f1}^{i-1,j,k,L}}{2\Delta x_2} + \frac{v_{f2}^{i,j+1,k,L} - v_{f2}^{i,j-1,k,L}}{2\Delta x_1} \right) + \sigma_{f23}^{i,j,k,L} \left(\frac{v_{f2}^{i,j+1,k,L} - v_{f2}^{i,j-1,k,L}}{2\Delta x_3} + \frac{v_{f3}^{i,j,k+1,L} - v_{f3}^{i,j,k-1,L}}{2\Delta x_2} \right) \\
 &\quad + \sigma_{f31}^{i,j,k,L} \left(\frac{v_{f3}^{i+1,j,k,L} - v_{f3}^{i-1,j,k,L}}{2\Delta x_1} + \frac{v_{f1}^{i,j,k+1,L} - v_{f1}^{i,j,k-1,L}}{2\Delta x_3} \right), \\
 \left(\nabla_x \cdot (\mathbb{K}_f \cdot \nabla_x \theta_f) \right)^{i,j,k,L} &\approx \mathbb{K}_f^{i,j,k,L} \frac{\theta_f^{i+1,j,k,L} - 2\theta_f^{i,j,k,L} + \theta_f^{i-1,j,k,L}}{\Delta x_1^2} + \mathbb{K}_f^{i,j,k,L} \frac{\theta_f^{i,j+1,k,L} - 2\theta_f^{i,j,k,L} + \theta_f^{i,j-1,k,L}}{\Delta x_2^2} \\
 &\quad + \mathbb{K}_f^{i,j,k,L} \frac{\theta_f^{i,j,k+1,L} - 2\theta_f^{i,j,k,L} + \theta_f^{i,j,k-1,L}}{\Delta x_3^2}
 \end{aligned} \tag{3.3}$$

and for the balance of linear momentum

$$\begin{aligned}
 \left(\frac{\partial v_{f1}}{\partial t} \right)^{i,j,k,L} &\approx \frac{v_{f1}^{i,j,k,L} - v_{f1}^{i,j,k,L-1}}{\Delta t}, \quad \left(\frac{\partial v_{f2}}{\partial t} \right)^{i,j,k,L} \approx \frac{v_{f2}^{i,j,k,L} - v_{f2}^{i,j,k,L-1}}{\Delta t}, \quad \left(\frac{\partial v_{f3}}{\partial t} \right)^{i,j,k,L} \approx \frac{v_{f3}^{i,j,k,L} - v_{f3}^{i,j,k,L-1}}{\Delta t}, \\
 \left((\nabla_x \mathbf{v}_f) \cdot \mathbf{v}_f \right)^{i,j,k,L} &\approx v_{f1}^{i,j,k,L} \frac{v_{f1}^{i+1,j,k,L} - v_{f1}^{i-1,j,k,L}}{2\Delta x_1} + v_{f2}^{i,j,k,L} \frac{v_{f1}^{i,j+1,k,L} - v_{f1}^{i,j-1,k,L}}{2\Delta x_2} + v_{f3}^{i,j,k,L} \frac{v_{f1}^{i,j,k+1,L} - v_{f1}^{i,j,k-1,L}}{2\Delta x_3} \\
 &\quad + v_{f1}^{i,j,k,L} \frac{v_{f2}^{i+1,j,k,L} - v_{f2}^{i-1,j,k,L}}{2\Delta x_1} + v_{f2}^{i,j,k,L} \frac{v_{f2}^{i,j+1,k,L} - v_{f2}^{i,j-1,k,L}}{2\Delta x_2} + v_{f3}^{i,j,k,L} \frac{v_{f2}^{i,j,k+1,L} - v_{f2}^{i,j,k-1,L}}{2\Delta x_3} \\
 &\quad + v_{f1}^{i,j,k,L} \frac{v_{f3}^{i+1,j,k,L} - v_{f3}^{i-1,j,k,L}}{2\Delta x_1} + v_{f2}^{i,j,k,L} \frac{v_{f3}^{i,j+1,k,L} - v_{f3}^{i,j-1,k,L}}{2\Delta x_2} + v_{f3}^{i,j,k,L} \frac{v_{f3}^{i,j,k+1,L} - v_{f3}^{i,j,k-1,L}}{2\Delta x_3}, \\
 \left(\nabla_x \cdot \boldsymbol{\sigma}_f \right)^{i,j,k,L} &\approx \left(\frac{\sigma_{f11}^{i+1,j,k,L} - \sigma_{f11}^{i-1,j,k,L}}{2\Delta x_1} + \frac{\sigma_{f12}^{i,j+1,k,L} - \sigma_{f12}^{i,j-1,k,L}}{2\Delta x_2} + \frac{\sigma_{f13}^{i,j,k+1,L} - \sigma_{f13}^{i,j,k-1,L}}{2\Delta x_3} \right) \mathbf{e}_1 \\
 &\quad + \left(\frac{\sigma_{f21}^{i+1,j,k,L} - \sigma_{f21}^{i-1,j,k,L}}{2\Delta x_1} + \frac{\sigma_{f22}^{i,j+1,k,L} - \sigma_{f22}^{i,j-1,k,L}}{2\Delta x_2} + \frac{\sigma_{f23}^{i,j,k+1,L} - \sigma_{f23}^{i,j,k-1,L}}{2\Delta x_3} \right) \mathbf{e}_2 \\
 &\quad + \left(\frac{\sigma_{f31}^{i+1,j,k,L} - \sigma_{f31}^{i-1,j,k,L}}{2\Delta x_1} + \frac{\sigma_{f32}^{i,j+1,k,L} - \sigma_{f32}^{i,j-1,k,L}}{2\Delta x_2} + \frac{\sigma_{f33}^{i,j,k+1,L} - \sigma_{f33}^{i,j,k-1,L}}{2\Delta x_3} \right) \mathbf{e}_3.
 \end{aligned} \tag{3.4}$$

The discretized system is formulated next as an implicit time-stepping scheme within each time-step L , whereby (1) one solves for the density, assuming the thermal and velocity fields fixed, (2) one solves for the temperature, assuming the

density and velocity fields fixed, then (3) one solves for the velocity, assuming the density and thermal fields fixed. Below, we formulate such a system, with an iterative counter K (within a time-step), for each finite difference node

$$\begin{aligned} \rho_f^{i,j,k,L+1,K} &= \rho_f^{i,j,k,L} - \Delta t (\nabla_x \cdot (\rho_f \mathbf{v}_f))^{i,j,k,L+1,K-1}, \\ \mathcal{L}(\rho_f^{i,j,k,L+1,K-1}, \rho_f^{i,j,k,L+1,K}, \theta_f^{i,j,k,L+1,K-1}) &= 0, \\ \theta_f^{i,j,k,L+1,K} &= \theta_f^{i,j,k,L} - \Delta t (\nabla_x \theta_f \cdot \mathbf{v}_f)^{i,j,k,L+1,K-1} + \left(\frac{\Delta t}{\rho_f C_f} (\boldsymbol{\sigma}_f : \nabla_x \mathbf{v}_f + \nabla_x \cdot (\mathbb{K}_f \cdot \nabla_x \theta_f) + \rho_f z_f) \right)^{i,j,k,L+1,K-1}, \\ \mathbf{v}_f^{i,j,k,L+1,K} &= \mathbf{v}_f^{i,j,k,L} - \Delta t (\nabla_x \mathbf{v}_f \cdot \mathbf{v}_f)^{i,j,k,L+1,K-1} + \left(\frac{\Delta t}{\rho_f} (\nabla_x \cdot \boldsymbol{\sigma}_f + \rho_f \mathbf{b}_f) \right)^{i,j,k,L+1,K-1}. \end{aligned} \quad (3.5)$$

In an abstract setting, we have:

$$\begin{aligned} \mathcal{A}_{f1}(\underline{\rho_f^{L+1,K}}, \underline{\theta_f^{L+1,K-1}}, \underline{\mathbf{v}_f^{L+1,K-1}}) &= \mathcal{F}_{f1}(\rho_f^{L+1,K-1}, \theta_f^{L+1,K-1}, \mathbf{v}_f^{L+1,K-1} \dots) \quad (\text{CONTINUITY}), \\ \mathcal{A}_{f2}(\underline{\rho_f^{L+1,K}}, \underline{\theta_f^{L+1,K}}, \underline{\mathbf{v}_f^{L+1,K-1}}) &= \mathcal{F}_{f2}(\rho_f^{L+1,K}, \theta_f^{L+1,K-1}, \mathbf{v}_f^{L+1,K-1} \dots) \quad (\text{ENERGY}), \\ \mathcal{A}_{f3}(\underline{\rho_f^{L+1,K}}, \underline{\theta_f^{L+1,K}}, \underline{\mathbf{v}_f^{L+1,K}}) &= \mathcal{F}_{f3}(\rho_f^{L+1,K}, \theta_f^{L+1,K}, \mathbf{v}_f^{L+1,K-1} \dots) \quad (\text{MOMENTUM}), \end{aligned} \quad (3.6)$$

where only the underlined variable is active (to be solved for) in the corresponding differential equation.

4. Numerical discretization of the particle equations

For the time discretization of the acceleration terms in the equations of motion (Eq. (2.1)), for each particle, one writes

$$\ddot{\mathbf{r}}^{L+1} \approx \frac{\dot{\mathbf{r}}^{L+1} - \dot{\mathbf{r}}^L}{\Delta t} \approx \frac{\frac{\mathbf{r}^{L+1} - \mathbf{r}^L}{\Delta t} - \dot{\mathbf{r}}^L}{\Delta t} \approx \frac{\mathbf{r}^{L+1} - \mathbf{r}^L}{\Delta t^2} - \frac{\dot{\mathbf{r}}^L}{\Delta t}, \quad (4.1)$$

which collapses to the familiar difference stencil of $\ddot{\mathbf{r}}^{L+1} \approx \frac{\mathbf{r}^{L+1} - 2\mathbf{r}^L + \mathbf{r}^{L-1}}{(\Delta t)^2}$, when all the time-steps size are uniform. Inserting this into $m\ddot{\mathbf{r}} = \Psi^{\text{tot}}(\mathbf{r})$ leads to

$$\mathbf{r}^{L+1,K} \approx \frac{\Delta t^2}{m} (\Psi^{\text{tot}}(\mathbf{r}^{L+1,K-1})) + (\mathbf{r}^L + \Delta t \dot{\mathbf{r}}^L). \quad (4.2)$$

For the thermal behavior, after temporal integration with the previously used finite difference time-step (for the fluid), we have (from Eq. (4.1))

$$\theta(t + \Delta t) = \frac{mC}{mC + h_c a_s \Delta t} \theta(t) - \frac{\Delta t \mathcal{B} a_s \epsilon}{mC + h_c a_s \Delta t} (\theta^4(t + \Delta t) - \theta_s^4) + \frac{m c_v \Delta t |\mathbf{b}_D \cdot (\langle \mathbf{v}_f \rangle_\omega - \mathbf{v})|}{mC + h_c a_s \Delta t} + \frac{h_c a_s \Delta t \theta_0}{mC + h_c a_s \Delta t}. \quad (4.3)$$

This implicit nonlinear equation for θ , for each particle, is recast as

$$\theta^{L+1,K} = \frac{mC}{mC + h_c a_s \Delta t} \theta^L - \frac{\Delta t \mathcal{B} a_s \epsilon}{mC + h_c a_s \Delta t} ((\theta^{L+1,K-1})^4 - \theta_s^4) + \frac{m c_v \Delta t |\mathbf{b}_D \cdot (\langle \mathbf{v}_f^{L+1,K} \rangle_\omega - \mathbf{v}^{L+1,K})|}{mC + h_c a_s \Delta t} + \frac{h_c a_s \Delta t \theta_0}{mC + h_c a_s \Delta t} \quad (4.4)$$

and is added into the fixed-point scheme with the equations of momentum balance and the equations governing the fluid mechanics. Concisely, the equations for the particle mechanics problem can be addressed in an abstract setting, whereby one solves for the particle positions, assuming the thermal fields fixed:

$$\mathcal{A}_{p1}(\underline{\mathbf{r}^{L+1,K}}, \underline{\theta^{L+1,K-1}}) = \mathcal{F}_{p1}(\mathbf{r}^{L+1,K-1}, \theta^{L+1,K-1}), \quad (4.5)$$

then one solves for the thermal fields, assuming the particle positions fixed,

$$\mathcal{A}_{p2}(\underline{\mathbf{r}^{L+1,K}}, \underline{\theta^{L+1,K}}) = \mathcal{F}_{p2}(\mathbf{r}^{L+1,K}, \theta^{L+1,K-1}). \quad (4.6)$$

Both of these equations, and the equations for the fluid, are solved simultaneously with an *adaptive multifield* staggering scheme, which we discuss shortly.

Remarks: In order to determine the thermal state of the particles when impact-induced reactions are significant, we shall decompose the heat generation and heat transfer processes into two stages. Stage I describes the extremely short time interval when impact occurs, $\delta t \ll \Delta t$, and accounts for the effects of chemical reactions, which are relevant in certain applications, and energy release due to mechanical straining. Stage II accounts for the post impact behavior involving convective and radiative effects, as discussed earlier. As before, we consider an energy balance, governing the interconversions of mechanical, thermal and chemical energy in a system, dictated by the First Law of Thermodynamics, $\frac{d}{dt}(\mathcal{K} + \mathcal{S}) = \mathcal{P} + \mathcal{H}$, with the previous assumptions leading to $\frac{d\mathcal{E}}{dt} = \mathcal{H}$. For Stage I, the primary source of heat is the chemical reactions that occur upon impact, due to the presence of a reactive layer. The chemical reaction energy is defined as

$$\delta \mathcal{H} \stackrel{\text{def}}{=} \int_t^{t+\delta t} \mathcal{H} \, dt. \tag{4.7}$$

Eq. (2.8) can be rewritten for the temperature at time = $t + \delta t$ as

$$\theta(t + \delta t) = \theta(t) + \frac{\delta \mathcal{H}}{mC}. \tag{4.8}$$

The energy released from the reactions is assumed to be proportional to the amount of the fluid substance (for example a gas) available to be compressed in the contact area between the particles. A typical, ad-hoc approximation in combustion processes is to write, for example, a linear relation, with a saturation (limiting) value (ξ),

$$\delta \mathcal{H} \approx \xi \min \left(\frac{|\bar{I}_n|}{I_n^*}, 1 \right) \pi b^2, \tag{4.9}$$

where ξ is the reaction constant (energy per unit area [J/m^2]), I_n^* is a normalization parameter and b is the particle radius. For details on a variety of such relations of this type see, for example, Schmidt [77]. For the particle sizes and material properties of interest, the term, $\frac{\delta \mathcal{H}}{mC}$, in Eq. (4.8) indicates that

$$\delta \theta \stackrel{\text{def}}{=} \theta(t + \delta t) - \theta(t) = \frac{\delta \mathcal{H}}{mC} \propto \frac{\xi}{\rho C b}. \tag{4.10}$$

Thus, when values of ξ are chosen such that $\frac{\xi}{\rho C b} \gg 1$, this will generate significant amount of heat.¹³ Thereafter (Stage II, post-impact), it is assumed that a process of convection, for example governed by Newton’s law of cooling, and radiation according to a simple Stefan–Boltzmann law transpires. Since $\delta t \ll \Delta t$ we assign $\bar{\theta}^L = \theta(t + \delta t) = \theta(t) + \frac{\delta \mathcal{H}}{mC}$ and replace θ^L with it in Eq. (4.4) to obtain

$$\theta^{L+1,K} = \frac{mC}{mC + h_c a_s \Delta t} \bar{\theta}^L - \frac{\Delta t \mathcal{B} a_s \epsilon}{mC + h_c a_s \Delta t} ((\theta^{L+1,K-1})^4 - \theta_s^4) + \frac{m c_v \Delta t |\mathbf{b}_D \cdot ((\mathbf{v}_f^{L+1,K})_\omega - \mathbf{v}^{L+1,K})|}{mC + h_c a_s \Delta t} + \frac{h_c a_s \Delta t \theta_0}{mC + h_c a_s \Delta t}. \tag{4.11}$$

5. An adaptive staggering solution scheme

We now develop a temporally-adaptive staggering scheme by extending an approach found in Zohdi [94–97]. Broadly speaking, staggering schemes proceed by solving each field equation individually, allowing only the primary field variable to be active. After the solution of each field equation, the primary field variable is updated, and the next field equation is addressed in a similar manner. Such approaches have a long history in the computational mechanics community. For example, see Schrefler [78], Zienkiewicz [93], Lewis et al. [54] and Lewis and Schrefler [53]. Park and Felippa [70], Piperno [71], Le Tallec and Mouro [52], Doltsinis [26,27] and the extensive works of Farhat and coworkers [72,32,51,33,73,34].

5.1. Analysis of the fluid/particle system

Let us denote the entire coupled system as $\mathcal{A}(\mathbf{w}^{L+1}) = \mathcal{F}$, where \mathbf{w} is a multifield vector that represents the particle positions (\mathbf{r}), the particle temperatures (θ), the nodal fluid velocities (\mathbf{v}_f) and temperatures (θ_f), i.e. $\mathbf{w} = (\mathbf{r}, \theta, \mathbf{v}_f, \theta_f)$. It is convenient to write

$$\mathcal{A}(\mathbf{w}^{L+1}) - \mathcal{F} = \mathcal{G}(\mathbf{w}^{L+1}) - \mathbf{w}^{L+1} + \mathcal{R} = \mathbf{0}, \tag{5.1}$$

where \mathcal{R} is a remainder term which does not depend on the solution, i.e. $\mathcal{R} \neq \mathcal{R}(\mathbf{w}^{L+1})$. A straightforward iterative scheme can be written as

$$\mathbf{w}^{L+1,K} = \mathcal{G}(\mathbf{w}^{L+1,K-1}) + \mathcal{R}. \tag{5.2}$$

The convergence of such a scheme is dependent on the characteristics of \mathcal{G} . Namely, a sufficient condition for convergence is that \mathcal{G} is a contraction mapping for all $\mathbf{w}^{L+1,K}$, $K = 1, 2, 3, \dots$. In order to investigate this further, we define the staggering error as $\mathcal{E}^{L+1,K} = \mathbf{w}^{L+1,K} - \mathbf{w}^{L+1}$. A necessary restriction for convergence is iterative self consistency, i.e. the “exact” (staggering error free) solution must be represented by the scheme $\mathcal{G}(\mathbf{w}^{L+1}) + \mathcal{R} = \mathbf{w}^{L+1}$. Enforcing this restriction, a sufficient condition for convergence is the existence of a contraction mapping of the form can be written

$$\|\mathcal{E}^{L+1,K}\| = \|\mathbf{w}^{L+1,K} - \mathbf{w}^{L+1}\| = \|\mathcal{G}(\mathbf{w}^{L+1,K-1}) - \mathcal{G}(\mathbf{w}^{L+1})\| \leq \eta \|\mathbf{w}^{L+1,K-1} - \mathbf{w}^{L+1}\|, \tag{5.3}$$

¹³ By construction, this model has increased heat production, via $\delta \mathcal{H}$, as κ increases.

where, if $\eta < 1$ for each iteration K , then $\mathcal{E}^{L+1,K} \rightarrow \mathbf{0}$ for any arbitrary starting value $\mathbf{w}^{L+1,K=0}$ as $K \rightarrow \infty$. This contraction condition is sufficient, but not necessary, for convergence. For example, if we isolate the equation for the dynamics of the particles,

$$\mathbf{r}^{L+1,K} \approx \underbrace{\frac{\Delta t^2}{m} (\Psi^{\text{tot}}(\mathbf{r}^{L+1,K-1}))}_{\mathcal{G}(\mathbf{r}^{L+1,K-1})} + \underbrace{(\mathbf{r}^L + \Delta t \dot{\mathbf{r}}^L)}_{\mathcal{R}}, \tag{5.4}$$

we observe that convergence is restricted by $\eta \propto EIG(\mathcal{G}) \propto \frac{\Delta t^2}{m}$. Thus, decreasing the time-step size improves the convergence, however, we want to simultaneously maximize the time-step sizes to decrease overall computing time, while still meeting an error tolerance. In order to achieve this goal, we follow an approach in Zohdi [94,95] initially developed for continuum thermo-chemical multifield problems in which (1) one approximates $\eta \approx S(\Delta t)^p$ (S is a constant) and (2) one assumes that the error within an iteration behaves approximately according to $(S(\Delta t)^p)^K \|\mathcal{E}^{L+1,0}\| = \|\mathcal{E}^{L+1,K}\|$, $K = 1, 2, \dots$, where $\|\mathcal{E}^{L+1,0}\|$ is the initial norm of the iterative error and S is a function intrinsic to the system.¹⁴ Our goal is to meet an error tolerance in exactly a preset number of iterations. To this end, one writes this in the following approximate form, $(S(\Delta t_{\text{tol}})^p)^{K_d} \|\mathcal{E}^{L+1,0}\| = \text{TOL}$, where TOL is a tolerance and where K_d is the number of desired iterations.¹⁵ If the error tolerance is not met in the desired number of iterations, the contraction constant η is too large. Accordingly, one can solve for a new smaller step size, under the assumption that S is constant,¹⁶

$$\Delta t_{\text{tol}} = \Delta t \left(\frac{\left(\frac{\text{TOL}}{\|\mathcal{E}^{L+1,0}\|} \right)^{\frac{1}{K_d}}}{\left(\frac{\|\mathcal{E}^{L+1,K}\|}{\|\mathcal{E}^{L+1,0}\|} \right)^{\frac{1}{K}}} \right). \tag{5.5}$$

The assumption that S is constant is not critical, since the time-steps are to be recursively refined and unrefined repeatedly. Clearly, the previous expression can also be used for time-step enlargement, if convergence is met in less than K_d iterations. Time-step size adaptivity is paramount, since the flow’s dynamics can dramatically change over the course of time, requiring radically different time-step sizes for a preset level of accuracy. However, one must respect an upper bound dictated by the discretization error, i.e., $\Delta t \leq \Delta t^{\text{lim}}$. In order to couple this to the multifield computations, we define the normalized errors within each time-step, for the particles (summing over all particles)

$$\mathcal{E}_{rK} \stackrel{\text{def}}{=} \frac{\|\mathbf{r}^{L+1,K} - \mathbf{r}^{L+1,K-1}\|}{\|\mathbf{r}^{L+1,K} - \mathbf{r}^L\|} \quad \text{and} \quad \mathcal{E}_{\theta K} \stackrel{\text{def}}{=} \frac{\|\theta^{L+1,K} - \theta^{L+1,K-1}\|}{\|\theta^{L+1,K} - \theta^L\|} \tag{5.6}$$

and for the fluid (summing over all of the finite difference nodes)

$$\hat{\mathcal{E}}_{r_f K} \stackrel{\text{def}}{=} \frac{\|\mathbf{v}_f^{L+1,K} - \mathbf{v}_f^{L+1,K-1}\|}{\|\mathbf{v}_f^{L+1,K} - \mathbf{v}_f^L\|} \quad \text{and} \quad \hat{\mathcal{E}}_{\theta_f K} \stackrel{\text{def}}{=} \frac{\|\theta_f^{L+1,K} - \theta_f^{L+1,K-1}\|}{\|\theta_f^{L+1,K} - \theta_f^L\|}. \tag{5.7}$$

One can interpret these error metrics as the ratio of the staggering error to the change in the actual solution (from time-step to time-step). We now combine all of these (normalized) error metrics (ratios) into one single measure

$$\mathcal{E}_{\text{tot},K} = \frac{w_1 \mathcal{E}_{rK} + w_2 \mathcal{E}_{\theta K} + w_3 \hat{\mathcal{E}}_{r_f K} + w_4 \hat{\mathcal{E}}_{\theta_f K}}{w_1 + w_2 + w_3 + w_4}, \tag{5.8}$$

where the w_i ’s are weights. The overall algorithm is as follows:

¹⁴ For the class of problems under consideration, due to the quadratic dependency on Δt , $p \approx 2$.
¹⁵ Typically, K_d is chosen to be between 5 and 10 iterations.
¹⁶ In the definition of the error, since the “true” solution at a time-step, \mathbf{w}^{L+1} , is unknown, we use the most current value of the solution, $\mathbf{w}^{L+1,K}$, thus the error is to be interpreted as the relative error.

(0) GLOBAL FIXED – POINT ITERATION : (SET $i = 1$ AND $K = 0$) :

(1) COMPUTE FLUID SOLUTION (FOR EACH NODE) : $(\mathbf{v}_f, \rho_f, \theta_f)^{L+1, K}$ (FREEZING PARTICLE POSITIONS)

(2) IF $i > N_p$ THEN GO TO (4)

(3) IF $i \leq N_p$ THEN : (FREEZING FLUID VARIABLES)

(a) COMPUTE POSITION : $\mathbf{r}_i^{L+1, K} = \frac{\Delta t^2}{m_i} (\Psi_i^{tot}(\mathbf{r}^{L+1, K-1})) + \mathbf{r}_i^L + \Delta t \dot{\mathbf{r}}_i^L$

(b) COMPUTE TEMPERATURE :

$$\theta_i^{L+1, K} = \frac{mC}{mC + h_c a_s \Delta t} \theta_i^{L+1, K-1} - \frac{\Delta t B a_s \epsilon}{mC + h_c a_s \Delta t} ((\theta_i^{L+1, K-1})^4 - \theta_s^4)$$

$$+ \frac{h_c a_s \Delta t \theta_o}{mC + h_c a_s \Delta t} + \frac{m c_v \Delta t |b_D \cdot ((\mathbf{v}_f^{L+1, K})_{\omega_i} - \mathbf{v}^{L+1, K})|}{mC + h_c a_s \Delta t}$$

(c) GO TO (2) AND NEXT FLOW PARTICLE ($i = i + 1$)

(4) ERROR MEASURES :

(a) $\mathcal{E}_{rK} \stackrel{\text{def}}{=} \frac{\sum_{i=1}^{N_p} \|\mathbf{r}_i^{L+1, K} - \mathbf{r}_i^{L+1, K-1}\|}{\sum_{i=1}^{N_p} \|\mathbf{r}_i^{L+1, K} - \mathbf{r}_i^L\|}$ $\mathcal{E}_{\theta K} \stackrel{\text{def}}{=} \frac{\sum_{i=1}^{N_p} \|\theta_i^{L+1, K} - \theta_i^{L+1, K-1}\|}{\sum_{i=1}^{N_p} \|\theta_i^{L+1, K} - \theta_i^L\|}$

$\hat{\mathcal{E}}_{r_f K} \stackrel{\text{def}}{=} \frac{\|\mathbf{v}_f^{L+1, K} - \mathbf{v}_f^{L+1, K-1}\|}{\|\mathbf{v}_f^{L+1, K} - \mathbf{v}_f^L\|}$ $\hat{\mathcal{E}}_{\theta_f K} \stackrel{\text{def}}{=} \frac{\|\theta_f^{L+1, K} - \theta_f^{L+1, K-1}\|}{\|\theta_f^{L+1, K} - \theta_f^L\|}$

(b) $\mathcal{E}_{tot, K} = \frac{w_1 \mathcal{E}_{rK} + w_2 \mathcal{E}_{\theta K} + w_3 \hat{\mathcal{E}}_{r_f K} + w_4 \hat{\mathcal{E}}_{\theta_f K}}{w_1 + w_2 + w_3 + w_4}$ $TOL_{tot} = \frac{w_1 TOL_r + w_2 TOL_\theta + w_3 TOL_{r_f} + w_4 TOL_{\theta_f}}{w_1 + w_2 + w_3 + w_4}$

(c) $\Phi_K \stackrel{\text{def}}{=} \left(\frac{(TOL_{tot})^{\frac{1}{pK_d}}}{(\mathcal{E}_{tot, 0})^{\frac{1}{pK}}} \right)$

(5) IF TOLERANCE MET ($\mathcal{E}_{tot, K} \leq 1$) AND $K < K_d$ THEN :

(a) INCREMENT TIME : $t = t + \Delta t$

(b) CONSTRUCT NEW TIME STEP : $\Delta t = \Phi_K \Delta t$,

(c) SELECT MINIMUM : $\Delta t = \min(\Delta t^{lim}, \Delta t)$ AND GO TO (0)

(6) IF TOLERANCE NOT MET ($\mathcal{E}_{tot, K} > TOL$) AND $K = K_d$ THEN :

(a) CONSTRUCT NEW TIME STEP : $\Delta t = \Phi_K \Delta t$

(b) RESTART AT TIME = t AND GO TO (0).

(5.9)

The purpose of the algorithm is to deliver solutions where the coupling is resolved in an iterative manner, by the recursive staggered solution of the various field equations, constraints, etc. The incomplete coupling error is controlled by adaptively adjusting the time-step sizes, while the temporal discretization accuracy dictates the upper limit on the time-step size (Δt^{lim}).

Remark 1. In Box 5.9, at the implementation level, normalized (non-dimensional) error measures were used. As with the unnormalized case, one approximates the error within an iteration to behave according to

$$(S(\Delta t)^p)^K \underbrace{\frac{\|\mathbf{r}^{L+1, 1} - \mathbf{r}^{L+1, 0}\|}{\|\mathbf{r}^{L+1, 0} - \mathbf{r}^L\|}}_{\epsilon_0} = \underbrace{\frac{\|\mathbf{r}^{L+1, K} - \mathbf{r}^{L+1, K-1}\|}{\|\mathbf{r}^{L+1, K} - \mathbf{r}^L\|}}_{\epsilon_K}, \tag{5.10}$$

where the normalized measures characterize the ratio of the iterative (staggering) error within a time-step to the difference in solutions between time-steps. Since both $\|\mathbf{r}^{L+1, 0} - \mathbf{r}^L\| \approx \mathcal{O}(\Delta t)$ and $\|\mathbf{r}^{L+1, K} - \mathbf{r}^L\| \approx \mathcal{O}(\Delta t)$ are of the same order, the use of normalized or unnormalized measures makes little difference in rates of convergence. However, the normalized measures are preferred since they have a clearer interpretation.

Remark 2. We remark that the forces needed to compute terms in the coefficient of restitution e , for example E_{in} , E_{jn} and D_{ij} are obtained by using the most currently known values of the Ψ_i 's during the iterative solution process. In other words, the interaction forces are updated during the iterations, within a time-step, based on the most currently known positions of the particles. This process includes checking whether $\|\mathbf{r}_i - \mathbf{r}_j\| \leq b_i + b_j$, which is a criteria for contact between particles.

Remark 3. For the fluid, notice that all of the contraction factors in Eq. (3.6) scale as $\frac{\Delta t}{h}$ and $\frac{\Delta t}{h^2}$ (classical stability terms).

Remark 4. An alternative and more severe way to measure the error is to define “violation ratios”, i.e. measure of which field is relatively more in error, compared to its corresponding tolerance, via $Z_K \stackrel{\text{def}}{=} \max(z_{rK}, z_{\theta K}, \hat{z}_{vK}, \hat{z}_{\theta K})$ where

$$z_{rK} \stackrel{\text{def}}{=} \frac{\mathcal{E}_{rK}}{\text{TOL}_r} \quad \text{and} \quad z_{\theta K} \stackrel{\text{def}}{=} \frac{\mathcal{E}_{\theta K}}{\text{TOL}_\theta} \tag{5.11}$$

and

$$\hat{z}_{vK} \stackrel{\text{def}}{=} \frac{\hat{\mathcal{E}}_{vK}}{\text{TOL}_v} \quad \text{and} \quad \hat{z}_{\theta_r K} \stackrel{\text{def}}{=} \frac{\hat{\mathcal{E}}_{\theta_r K}}{\text{TOL}_{\theta_r}} \tag{5.12}$$

and then a minimum scaling factor $\Phi_K \stackrel{\text{def}}{=} \min(\phi_{rK}, \phi_{\theta K}, \hat{\phi}_{vK}, \hat{\phi}_{\theta_r K})$, where, for the particles

$$\phi_{rK} \stackrel{\text{def}}{=} \left(\frac{\left(\frac{\text{TOL}_r}{\mathcal{E}_{r0}} \right)^{\frac{1}{pK_d}}}{\left(\frac{\mathcal{E}_{rK}}{\mathcal{E}_{r0}} \right)^{\frac{1}{pK}}} \right), \quad \phi_{\theta K} \stackrel{\text{def}}{=} \left(\frac{\left(\frac{\text{TOL}_\theta}{\mathcal{E}_{\theta 0}} \right)^{\frac{1}{pK_d}}}{\left(\frac{\mathcal{E}_{\theta K}}{\mathcal{E}_{\theta 0}} \right)^{\frac{1}{pK}}} \right) \tag{5.13}$$

and for the fluid

$$\hat{\phi}_{vK} \stackrel{\text{def}}{=} \left(\frac{\left(\frac{\text{TOL}_v}{\hat{\mathcal{E}}_{v0}} \right)^{\frac{1}{pK_d}}}{\left(\frac{\hat{\mathcal{E}}_{vK}}{\hat{\mathcal{E}}_{v0}} \right)^{\frac{1}{pK}}} \right), \quad \hat{\phi}_{\theta_r K} \stackrel{\text{def}}{=} \left(\frac{\left(\frac{\text{TOL}_{\theta_r}}{\hat{\mathcal{E}}_{\theta_r 0}} \right)^{\frac{1}{pK_d}}}{\left(\frac{\hat{\mathcal{E}}_{\theta_r K}}{\hat{\mathcal{E}}_{\theta_r 0}} \right)^{\frac{1}{pK}}} \right). \tag{5.14}$$

However, in such an approach, if the individual field with the maximum error is used for time-step adaptivity, we would need to specifically use the corresponding convergence exponent (p) for the selected field’s temporal discretization. If the equations of dynamic equilibrium of the particles are the field chosen, then $p = 2$. If the equations of thermodynamic equilibrium of the particles are the field chosen, then $p = 1$. If the equations of dynamic equilibrium of the fluid are the field chosen, then $p = 1$. If the equations of thermodynamic equilibrium of the fluid are the field chosen, then $p = 1$. However, this approach has some major drawbacks when many disparate fields are present. Specifically, when the maximum error measure oscillates from field to field within a time-step or abruptly from time-step to time-step, convergence becomes quite difficult. Using the combined metric (Eq. (5.8)) is more stable and, thus, preferred.

Remark 5. Crucial to the analysis is the observation that the convergence of such staggering schemes is generally proportional to the time-step size. An illustrative semi-analytical example is provided in Appendix B.

6. A numerical example

As a model problem, we considered a cubical representative volume of a particle-laden fluid flow (Fig. 2). The classical random sequential addition (RSA) algorithm was used to initially place non-overlapping spherical particles into the domain of interest [90]. This algorithm was adequate for the volume fraction ranges of interest (under 30%), since the limit of the method is on the order of 38%. To achieve higher volume fractions, there are a variety of more sophisticated meth-

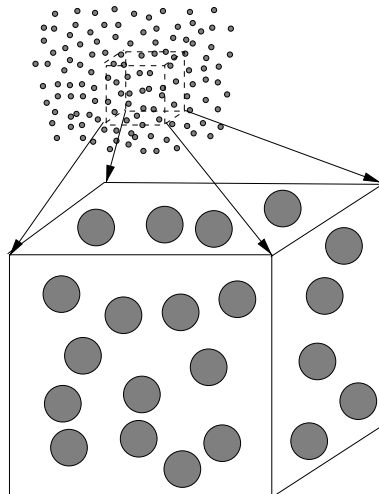


Fig. 2. A representative volume element extracted from a flow.

ods, such as those built upon the classical equilibrium-based Metropolis algorithm. For a detailed review of a variety of such methods, see Torquato [85]. For much higher volume fractions, effectively packing (and “jamming”) particles to theoretical limits (approximately 74%), a novel class of methods has recently been developed, based on simultaneous particle flow and growth, by Torquato and coworkers (see, for example, Kansaal et al. [46] and Donev et al. [28–30]). This class of methods was not employed in the present study, due to the relatively moderate volume fraction range of interest here, however, such methods appear to offer distinct computational advantages if extremely high volume fractions are desired.

Any particles that exited a boundary were given the same velocity (now incoming) on the opposite boundary. Periodicity conditions were used to generate any numerical derivatives for finite difference stencils that extended beyond the boundary. Clearly, under these conditions the group velocity of the particles will tend towards the velocity of the (“background”) fluid specified (controlled) on the boundary.

A Boussinesq-type (perturbation from an ideal gas) relation, adequate to describe dense gases and fluids, was used for the equation of state, stemming from

$$\rho_f \approx \rho_0(\theta_0, P_0) + \left. \frac{\partial \rho_f}{\partial P_f} \right|_{\theta} \Delta P_f + \left. \frac{\partial \rho_f}{\partial \theta_f} \right|_{P_f} \Delta \theta_f, \tag{6.1}$$

where ρ_0, θ_0, P_0 are reference values, $\Delta P_f = P_f - P_0$ and $\Delta \theta_f = \theta_f - \theta_0$. We define the thermal expansion as

$$\zeta_\theta \stackrel{\text{def}}{=} -\frac{1}{\rho_f} \left. \frac{\partial \rho_f}{\partial \theta_f} \right|_{P_f} = \frac{1}{V_f} \left. \frac{\partial V_f}{\partial \theta_f} \right|_{P_f} \tag{6.2}$$

and the bulk (compressibility) modulus by

$$\zeta_{\text{com}} \stackrel{\text{def}}{=} -V_f \left. \frac{\partial P_f}{\partial V_f} \right|_{\theta_f} = \rho_f \left. \frac{\partial P_f}{\partial \rho_f} \right|_{\theta_f}, \tag{6.3}$$

yielding the desired result

$$\rho_f \approx \rho_0 \left(1 - \zeta_\theta \Delta \theta_f + \frac{1}{\zeta_{\text{com}}} \Delta P_f \right), \tag{6.4}$$

leading to

$$P_f \approx P_0 + \zeta_{\text{com}} \left(\frac{\rho_f}{\rho_0} - 1 + \zeta_\theta \Delta \theta_f \right), \tag{6.5}$$

where $\mathcal{O}(\zeta_\theta) \approx 10^{-7}/K$ and $10^5 \text{ Pa} < \mathcal{O}(\zeta_{\text{com}}) < 10^{10} \text{ Pa}$. The viscosity is assumed to behave according to the well-known relation

$$\frac{\mu_f}{\mu_r} = e^{c \left(\frac{\theta_r}{\theta_f} - 1 \right)}, \tag{6.6}$$

where μ_r is a reference viscosity, θ_r is a reference temperature and where c is a material constant. We introduce the following (per unit *mass*²) decompositions for the key near-field parameters, for example for the force imparted on particle i by particle j and vice-versa¹⁷

- $\alpha_{1ij} = \bar{\alpha}_1 m_i m_j,$
- $\alpha_{2ij} = \bar{\alpha}_2 m_i m_j.$

One should expect two primary trends:

- Larger particles are more massive and can impact one another without significant influence from the surrounding fluid. In other words, the particles can “plow” through the fluid and make contact. This makes this situation more thermally volatile, due to the resulting chemical release at contact.
- Smaller particles are more sensitive to the surrounding fluid, and the drag ameliorates the disparity in velocities, thus minimizing the interparticle impact. Thus, these types of flows are less thermally sensitive.

Obviously, in such a model, the number of parameters, even though they are not ad hoc, is large. Thus, corresponding parameter studies would be enormous. This is not the objective of this paper. Accordingly, we have taken nominal

¹⁷ Alternatively, if the near-fields are related to the amount of surface area, this scaling could be done per unit area.

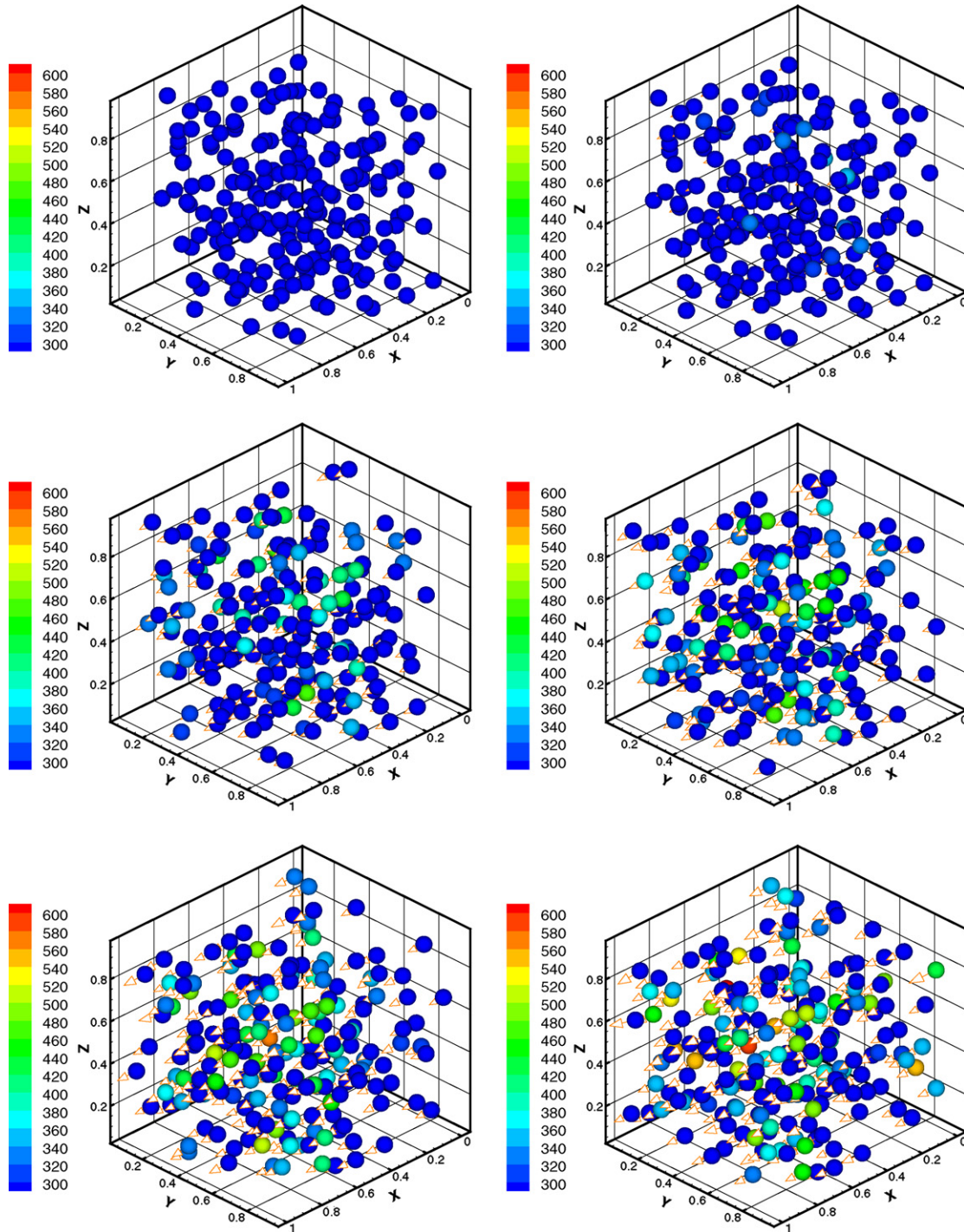


Fig. 3. *With near-fields* (top to bottom and left to right): the dynamics of the particulate flow. The lengths of the arrows indicate the magnitude of each particle's velocity.

parameter values that fall roughly in the middle of material data ranges to illustrate the basic approach. The parameters selected for the simulations were as follows:¹⁸

- a (normalized) domain size of $1\text{ m} \times 1\text{ m} \times 1\text{ m}$,
- 200 particles randomly distributed in the domain and all started from rest,

¹⁸ No gravitational effects were considered.

- the particle radii randomly distributed between $b = 0.05(1 \pm 0.25)$ m, this resulted in approximately 11% of the volume being occupied by the particles,
- an initial velocity of $\mathbf{v}_f = (1 \text{ m/s}, 0 \text{ m/s}, 0 \text{ m/s})$ was assigned to the fluid, and periodic boundary conditions were used,
- the viscosity parameters were $\mu_r = 0.05 \text{ N s/m}^2$ and $c = 5$, for the equation of state (Boussinesq-type model), and the same thermal relation is assumed for the bulk viscosity, namely, $\frac{\kappa_r}{\kappa_f} = e^{c\left(\frac{\theta_r}{\theta_f} - 1\right)}$, $\kappa_r = 0.8\mu_r$,¹⁹
- a uniform initial particle temperature of $\theta = 293.13 \text{ K}$ was used,
- a uniform initial fluid interior temperature of $\theta_f = 293.13 \text{ K}$ was used, and these values served as the boundary conditions for the domain,
- a particle heat capacity of $C = 1000 \text{ J/(kg K)}$,
- a fluid heat capacity of $C_f = 2500 \text{ J/(kg K)}$,
- a fluid conductivity of $K_f = 1.0 \text{ J m}^2/(\text{s K})$,
- a radiative particle emissivity of $\epsilon = 0.05$ was chosen,
- the near-field parameters for the particles were $\bar{\alpha}_1 = 0.1$, $\bar{\alpha}_2 = 0.01$, $\beta_1 = 1$, $\beta_2 = 2$,
- the restitution impact coefficients were $e^- = 0.1$ (the lower bound), $e_0 = 0.2$, $\theta^* = 3000 \text{ K}$ (thermal sensitivity coefficient), $v^* = 10 \text{ m/s}$,
- the coefficient of static friction was $\mu_s = 0.5$ and the coefficient of dynamic friction was $\mu_d = 0.2$,
- the reaction coefficient was $\zeta = 10^9 \text{ J/m}^2$ and the reaction impact parameter was $I^* = 10^3 \text{ N}$,
- the heat-drag coefficient, $c_v = 1$,
- the convective heat transfer coefficient was $h_c = 10^3 \text{ J/(s m}^2 \text{ K)}$,
- a bulk fluid (compressibility) modulus $\zeta_{\text{com}} = 10^6 \text{ Pa}$, the reference pressure $P_0 = 101,300 \text{ Pa}$ (1 atm), the reference density $\rho_0 = 1000 \text{ kg/m}^3$, reference temperature $\theta_0 = 293.13 \text{ K}$ and a thermal expansion coefficient, $\zeta_\theta = 10^{-7} (\text{K})^{-1}$,
- a particle density of $\rho = 2000 \text{ kg/m}^3$.

The discretization parameters selected were:

- a $10 \times 10 \times 10$ finite difference mesh (with a spacing of 0.1 m) for the numerical derivatives (on the order of the particle size),
- a simulation time of one second,
- an initial time-step size of 10^{-6} s ,
- an upper limit for the time-step size of 10^{-2} s ,
- a lower limit for the time-step size of 10^{-12} s ,
- a target number of internal fixed-point iterations of $K_d = 5$,
- an (percentage) iterative (normalized) relative error tolerance within a time-step was set to $\text{TOL}_1 = \text{TOL}_2 = \text{TOL}_3 = \text{TOL}_4 = 10^{-3}$.

7. Discussion of the results

For this system, the Reynolds number, based on the mean particle diameter and initial system parameters, was $Re \stackrel{\text{def}}{=} \frac{\rho_0 2bv_0}{\mu_0} \approx 4010$. The plots in Figs. 4 and 5 illustrate the system behavior with and without near-fields. There is significant heating due to interparticle collisions when near-fields are present. The presence of near-fields causes particle trajectories to intersect, due to mutual attraction and repulsion, and for the particles to make contact frequently. In other words, the particles can “plow” through the (compressible) fluid and contact one another. This makes this situation relatively more thermally volatile, due to the resulting chemical release at contact, than cases without near-fields, where the fluid dominates the motion of the particles relatively quickly, not allowing them to make contact. When no near-fields were present, the thermal changes in the particles were negligible, as the plots indicate (Fig. 5). A sequence of system configurations are shown in Fig. 3 for the case where near-fields are present. Referring to Table 1, the total number of time-steps needed was 1176 with near-fields and 1341 without near-fields, leading to an average size step size of $8.505 \times 10^{-4} \text{ s}$ with near-fields and $7.458 \times 10^{-4} \text{ s}$ without near-fields. The number of iterations needed per time-step was 6.978 with near-fields and 10.772 without near-fields. We note that while the target iteration limit was set to 5 iterations per time-step, the average value taken for a successful time-step exceeds this number, due to the fact that the adaptive algorithm frequently would have to “step back” during the time-step refinement process and restart the iterations with a smaller time-step. The step sizes varied between approximately $4.8 \times 10^{-4} \leq \Delta t \leq 1.1 \times 10^{-3} \text{ s}$ with near-fields and $4.8 \times 10^{-4} \leq \Delta t \leq 0.9 \times 10^{-3} \text{ s}$ without near-fields. In particular, it is important to note that, for the case with no near-fields, time-step adaptivity was important

¹⁹ In order to keep the analysis general, we do not enforce the Stokes’ condition, namely, $\kappa_f = 0$.

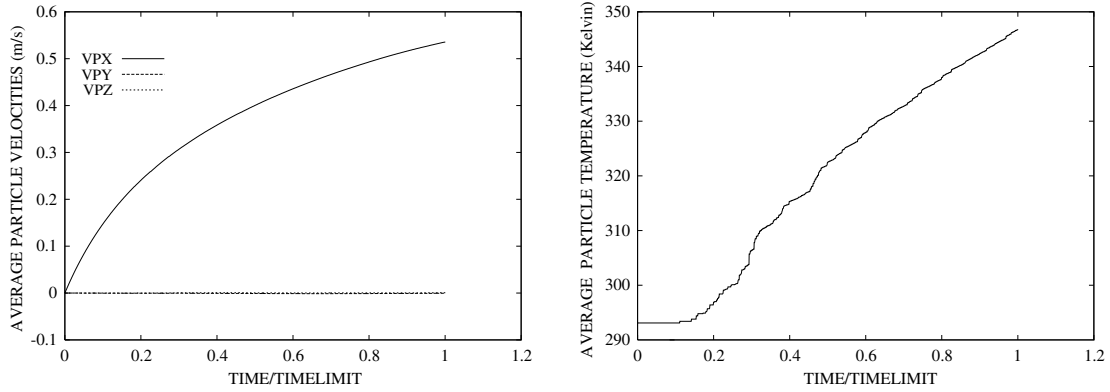


Fig. 4. With near-fields: The average velocity and temperature of the particles.

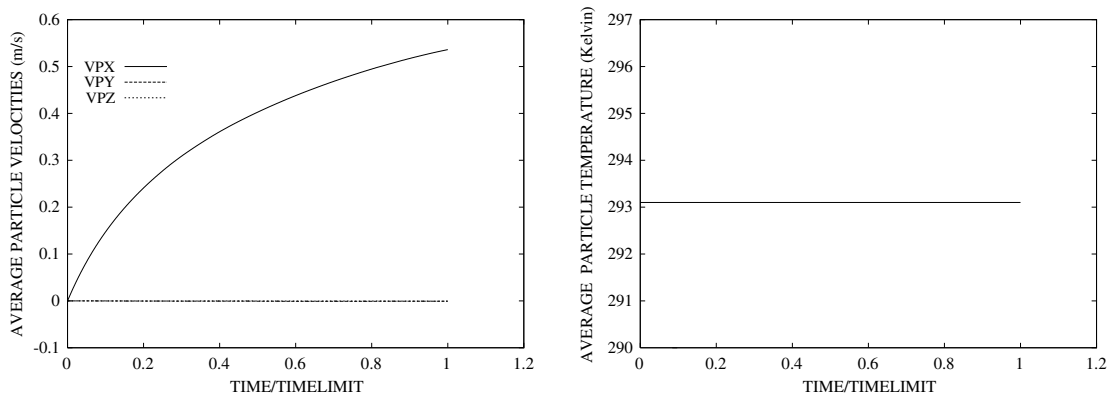


Fig. 5. Without near-fields: The average velocity and temperature of the particles.

Table 1
Statistics of the particle laden flow calculations

Near-field	Time-steps	Fixed-point iterations	Iter/time-steps	Time-step size (s)
Present	1176	8207	6.978	8.506×10^{-4}
Not present	1341	14,445	10.772	7.458×10^{-4}

throughout the simulation (Fig. 6). The near-field case’s computations converge more quickly. This appears to be due to the fact that when the near-fields are not present, the individual particles have a bit more mobility and, thus, smaller time-steps (slightly more computation) are needed to accurately capture their motion.

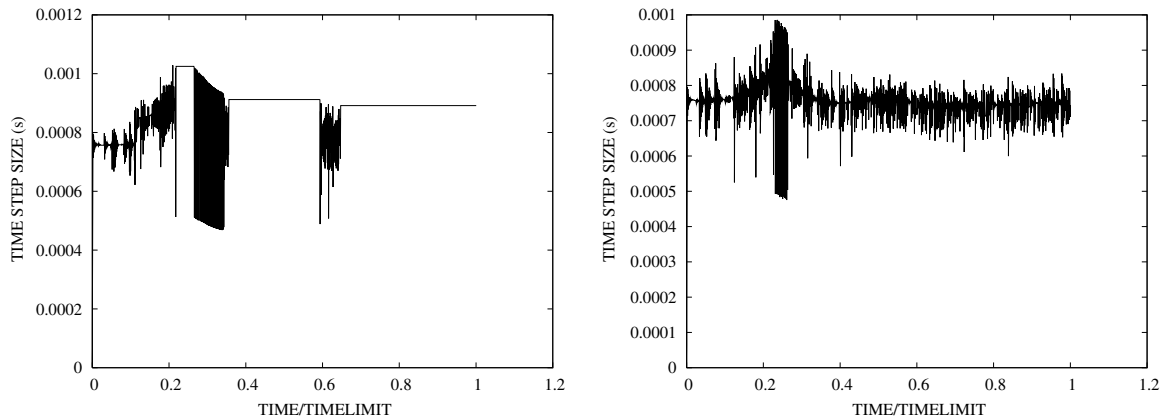


Fig. 6. The time-step size variation. On the left, with near-fields and, on the right, without near-fields.

8. Summary

This work developed a flexible and robust solution strategy to resolve strong multifield coupling between large numbers of particles and a surrounding fluid. As a model problem, a large number of particles undergoing inelastic collisions and simultaneous interparticle (non-local) near-field attraction/repulsion were considered. The particles were surrounded by a continuous interstitial fluid which was assumed to obey the compressible Navier–Stokes equations. Thermal effects were considered throughout the modeling and simulations. It was assumed that the particles were small enough that the effects of their rotation with respect to their mass centers was unimportant and that any “spin” of the particles was small enough to neglect lift forces that could arise from the interaction with the surrounding fluid. However, the particle–fluid system was strongly coupled due to the drag-forces induced by the fluid on the particles and vice-versa, as well as the generation of heat due to the drag-forces, thermal softening of the particles and the thermal dependency of the fluid viscosity. Because the coupling of the various particle and fluid fields can dramatically change over the course of a flow process, the focus of this work was on the development of an implicit “staggering” solution scheme, whereby the time-steps were adaptively adjusted to control the error associated with the incomplete resolution of the coupled interaction between the various solid particulate and continuum fluid fields. The approach is straightforward and can be easily incorporated within any standard computational fluid mechanics code based on finite difference, finite element or finite volume discretization. Furthermore, the presented staggering technique, which is designed to resolve the multifield coupling between particles and the surrounding fluid, can be used in a complementary way with other compatible approaches, for example those developed in the extensive works of Elghobashi and coworkers dealing with particle-laden and bubble-laden fluids [35,1,2,31]. Also, as mentioned earlier, improved descriptions of the fluid–particle interaction can possibly be achieved by using discrete network approximations such as those of Berlyand and Panchenko [15,16].

In closing, it is important to mention related particle-laden flow problems arising from the analysis of biological fluids. One application where problems of this type are encountered is in the study of atherosclerotic plaque growth. For example, a dominant school of thought attributes the inception of atherosclerotic plaque growth to a relatively high concentration of microscale suspensions (low-density lipoprotein (LDL) particles) in the diseased blood. The stages in the overall atherosclerotic plaque process appear to be (a) adhesion of monocytes (essentially, larger particulate suspensions) to the endothelial surface, which is controlled by the adhesion molecules stimulated by the excess LDL, the oxygen content and the intensity of the blood flow; (b) penetration of the monocytes into the intima and subsequent inflammation of the tissue; and (c) rupture of the plaque accompanied by some degree of thrombus formation or even subsequent occlusive thrombosis. Plaques with high risk of rupture are termed *vulnerable*, (see, for example, Fuster [37]). Currently, no adequate, robust, diagnostic strategy for the identification of vulnerable plaques is available. Surveys of the current thinking in the medical community pertaining to the growth and rupture of atherosclerotic plaques are provided in Shah [79], van der Wal [87], Chyu [22] and Libby [55–58], Richardson et al. [75] and Loree et al. [60], and Davies et al. [24], among others. For numerical and theoretical fluid flow analyses we refer the reader to Stroud et al. [81,82], Berger and Jou [14] and Jou and Berger [45]. For experimentally-oriented physiological flow studies of atherosclerotic carotid bifurcations and related systems, see Bale-Glickman et al. [4,5]. Notably, Bale-Glickman et al. [4,5] have constructed flow models which replicate the lumen of plaques excised intact from patients with severe atherosclerosis, which have shown that the complex internal geometry of the diseased artery, combined with the pulsatile input flows, gives exceedingly complex flow patterns. They have shown that the flows are highly three-dimensional and chaotic, with details varying from cycle to cycle. In particular, the vorticity and streamline maps confirm the highly complex and three-dimensional nature of the flow. The mechanisms involved in the initial stages of the disease, in particular stage (a), have not been extensively studied, although some simple semi-analytical qualitative studies have been carried out recently in Zohdi et al. [99] and Zohdi [100]. Clearly, the subsequent flow dynamics of the thrombus ejected by plaque rupture, and fragments thereof, comprised of aggregates of particles, is of interest in determining the chances for stroke. The particle/fluid modeling techniques developed in the present work are currently being applied to the mentioned biological problems by the author.

Appendix A. Near-field potentials

In order to motivate the concept of stability for such systems we refer to the classical theory of conservative forces. Here we summarize analyses given in Zohdi [96,98]. A force field Ψ^{nf} is said to be conservative if and only if there exists a continuously differentiable scalar field V such that $\Psi^{nf} = -\nabla V$. If the force field is conservative, with potential V , then a necessary and sufficient condition for a particle to be in equilibrium at that point is that $\Psi^{nf} = -\nabla V = \mathbf{0}$, in other words $\frac{\partial V}{\partial x_1} = 0$, $\frac{\partial V}{\partial x_2} = 0$ and $\frac{\partial V}{\partial x_3} = 0$. Forces acting on a particle that are in the direction of a vector connecting the center of the particle and a point, perhaps the center of another particle, and whose magnitude depend only on the distance between the particle and the point in question, are called *central forces*. The forces have the following form

$$\Psi^{nf} = -\mathcal{C}(\|\mathbf{r} - \mathbf{r}_0\|) \frac{\mathbf{r} - \mathbf{r}_0}{\|\mathbf{r} - \mathbf{r}_0\|} = \mathcal{C}(\|\mathbf{r} - \mathbf{r}_0\|)\mathbf{n}, \tag{A.1}$$

where \mathbf{r} is the position of the particle, where \mathbf{r}_0 is the position of the point of attraction/repulsion. The normal direction, connecting the two points, is given by $\mathbf{n} = \frac{\mathbf{r}_0 - \mathbf{r}}{\|\mathbf{r} - \mathbf{r}_0\|}$. The central force is one of attraction if $\mathcal{C}(\|\mathbf{r} - \mathbf{r}_0\|) > 0$ and one of repulsion if $\mathcal{C}(\|\mathbf{r} - \mathbf{r}_0\|) < 0$. We remark that a central force field is always conservative, since $\nabla \times \Psi^{nf} = \mathbf{0}$. For example, consider $V = \frac{\alpha_1 \|\mathbf{r} - \mathbf{r}_0\|^{-\beta_1 + 1}}{-\beta_1 + 1} - \frac{\alpha_2 \|\mathbf{r} - \mathbf{r}_0\|^{-\beta_2 + 1}}{-\beta_2 + 1}$, where all of the parameters, α 's and β 's, are non-negative. The gradient yields $-\nabla V = \Psi^{nf} = (\alpha_1 \|\mathbf{r} - \mathbf{r}_0\|^{-\beta_1} - \alpha_2 \|\mathbf{r} - \mathbf{r}_0\|^{-\beta_2})\mathbf{n}$, which is the form introduced previously. If a particle which is displaced slightly from an equilibrium point tends to return to that point, then we call that point a point of stability or stable point and the equilibrium is said to be stable. Otherwise we say that the point is one of instability and the equilibrium is unstable. *A necessary and sufficient condition that an equilibrium point be one of stability is that the potential V at the point be a minimum.* The general condition by which a potential is stable for the multidimensional case can be determined by studying the properties of the Hessian,

$$[\mathbb{H}] \stackrel{\text{def}}{=} \begin{bmatrix} \frac{\partial^2 V}{\partial x_1 \partial x_1} & \frac{\partial^2 V}{\partial x_1 \partial x_2} & \frac{\partial^2 V}{\partial x_1 \partial x_3} \\ \frac{\partial^2 V}{\partial x_2 \partial x_1} & \frac{\partial^2 V}{\partial x_2 \partial x_2} & \frac{\partial^2 V}{\partial x_2 \partial x_3} \\ \frac{\partial^2 V}{\partial x_3 \partial x_1} & \frac{\partial^2 V}{\partial x_3 \partial x_2} & \frac{\partial^2 V}{\partial x_3 \partial x_3} \end{bmatrix}, \tag{A.2}$$

around an equilibrium point. A sufficient condition for V to attain a minimum at an equilibrium point is that the Hessian be positive definite (which implies that V is locally convex). For more details see Hale and Kocak [42]. The central force potential chosen in this work is *near-field* stable for motion in the normal direction, i.e. the line connecting the centers of the particles. For disturbances in directions orthogonal to the normal direction, the potential is neutrally stable, i.e. the Hessian's determinant is zero, thus indicating that the potential does not change for such perturbations. Thus, in order to determine stable parameter combinations, consider a potential function for a single particle, in one-dimensional motion, representing the motion in the normal direction, attracted and repulsed from a point r_0 measured by the coordinate r ,

$$V = \frac{\alpha_1}{-\beta_1 + 1} |r - r_0|^{-\beta_1 + 1} - \frac{\alpha_2}{-\beta_2 + 1} |r - r_0|^{-\beta_2 + 1}, \tag{A.3}$$

whose derivative produces the form of interaction forces introduced earlier:

$$\Psi^{nf} = -\frac{\partial V}{\partial r} = \left(\alpha_1 |r - r_0|^{-\beta_1} - \alpha_2 |r - r_0|^{-\beta_2} \right) \mathbf{n}, \tag{A.4}$$

where $\mathbf{n} = \frac{\mathbf{r}_0 - \mathbf{r}}{\|\mathbf{r} - \mathbf{r}_0\|}$. We remark that the motion in the normal direction is relevant for central forces of this type. For stability, we require

$$\frac{\partial^2 V}{\partial r^2} = -\alpha_1 \beta_1 |r - r_0|^{-\beta_1 - 1} + \alpha_2 \beta_2 |r - r_0|^{-\beta_2 - 1} > 0. \tag{A.5}$$

A static equilibrium point, $r = r_e$, can be calculated from $\Psi^{nf}(|r_e - r_0|) = -\alpha_1 |r_e - r_0|^{-\beta_1} + \alpha_2 |r_e - r_0|^{-\beta_2} = 0$, which implies

$$|r_e - r_0| = \left(\frac{\alpha_2}{\alpha_1} \right)^{\frac{1}{-\beta_1 + \beta_2}}. \tag{A.6}$$

Inserting Eq. (A.6) into Eq. (A.5) yields a restriction for stability, $\frac{\beta_2}{\beta_1} > 1$.

One can consider the convexity requirement on the potential to insure that the perturbed motion to a dynamical state remain small. Consider the dynamics of a particle in the normal direction, with a perturbation, $\tilde{r} = r + \delta r$, $m\ddot{\tilde{r}} = \Psi^{nf}(\tilde{r})$, where r is the perturbation-free position vector of the particle, governed by $m\dot{r} = \Psi^{nf}(r)$. Taking the difference between these two differential equations yields

$$m\ddot{\delta r} = \Psi^{nf}(\tilde{r}) - \Psi^{nf}(r) \approx \frac{\partial \Psi^{nf}}{\partial r} \Big|_{\tilde{r}=r} \delta r + \dots \Rightarrow m\ddot{\delta r} - \frac{\partial \Psi^{nf}}{\partial r} \Big|_{\tilde{r}=r} \delta r \approx 0. \tag{A.7}$$

If $\frac{\partial \Psi^{nf}(r)}{\partial r}$ is positive, there will be exponential growth of the perturbation, while if $\frac{\partial \Psi^{nf}(r)}{\partial r}$ is negative, there will be oscillatory behavior of the perturbation. Thus, since $-\frac{\partial^2 V}{\partial r^2} = \frac{\partial \Psi^{nf}}{\partial r}$, we have

$$m\ddot{\delta r} + \frac{\partial^2 V}{\partial r^2} \Big|_{\tilde{r}=r} \delta r \approx 0. \tag{A.8}$$

The convexity of the potential simply corresponds to the positiveness of the stiffness at r . In addition to the instabilities about an equilibrium point, the point at which the potential changes from a convex to concave character is a source of long range instability. For motion in the normal direction, we have

$$\frac{\partial^2 V}{\partial r^2} = -\beta_1 \alpha_1 |r - r_0|^{-\beta_1 - 1} + \beta_2 \alpha_2 |r - r_0|^{-\beta_2 - 1} = 0, \tag{A.9}$$

thus leading to

$$|r - r_0| = \left(\frac{\beta_2 \alpha_2}{\beta_1 \alpha_1} \right)^{\frac{1}{-\beta_1 + \beta_2}} = d^*. \tag{A.10}$$

Thus, the preceding analysis indicates that, for the three-dimensional case, the interaction should be cut-off beyond $\|r_i - r_j\| = d^*$ to avoid long-range (central-force) instabilities.

Appendix B. A semi-analytical example of staggering schemes

To illustrate concepts, as an example, consider the coupling of two first-order equations and one second-order equation

$$a\dot{w}_1 + w_2 = 0, \quad b\dot{w}_2 + w_3 = 0, \quad c\ddot{w}_3 + w_1 = 0. \tag{B.1}$$

When the equations are discretized in time, for example with a backward Euler scheme, we obtain

$$\dot{w}_1^{L+1} = \frac{w_1^{L+1} - w_1^L}{\Delta t}, \quad \dot{w}_2^{L+1} = \frac{w_2^{L+1} - w_2^L}{\Delta t}, \quad \ddot{w}_3^{L+1} = \frac{w_3^{L+1} - 2w_3^L + w_3^{L-1}}{(\Delta t)^2}, \tag{B.2}$$

one obtains the following coupled system:

$$\begin{bmatrix} 1 & \frac{\Delta t}{a} & 0 \\ 0 & 1 & \frac{\Delta t}{b} \\ \frac{(\Delta t)^2}{c} & 0 & 1 \end{bmatrix} \begin{Bmatrix} w_1^{L+1} \\ w_2^{L+1} \\ w_3^{L+1} \end{Bmatrix} = \begin{Bmatrix} w_1^L \\ w_2^L \\ 2w_3^L - w_3^{L-1} \end{Bmatrix}. \tag{B.3}$$

For a recursive staggering scheme of Jacobi-type, where the updates are made only after one complete iteration, considered here only for algebraic simplicity, one has²⁰

$$\begin{bmatrix} 1 & 0 & 0 \\ 0 & 1 & 0 \\ 0 & 0 & 1 \end{bmatrix} \begin{Bmatrix} w_1^{L+1,K} \\ w_2^{L+1,K} \\ w_3^{L+1,K} \end{Bmatrix} = \begin{Bmatrix} w_1^L \\ w_2^L \\ 2w_3^L - w_3^{L-1} \end{Bmatrix} - \begin{Bmatrix} \frac{\Delta t}{a} w_1^{L+1,K-1} \\ \frac{\Delta t}{b} w_2^{L+1,K-1} \\ \frac{(\Delta t)^2}{c} w_3^{L+1,K-1} \end{Bmatrix}. \tag{B.4}$$

Rewriting this in terms of a standard “fixed-point” form, $\mathcal{G}(w^{L+1,K-1}) + \mathcal{R} = w^{L+1,K}$, yields

$$\underbrace{\begin{bmatrix} 0 & \frac{\Delta t}{a} & 0 \\ 0 & 0 & \frac{\Delta t}{b} \\ \frac{(\Delta t)^2}{c} & 0 & 0 \end{bmatrix}}_{\text{def } \mathcal{G}} \underbrace{\begin{Bmatrix} w_1^{L+1,K-1} \\ w_2^{L+1,K-1} \\ w_3^{L+1,K-1} \end{Bmatrix}}_{\text{def } w^{L+1,K-1}} + \underbrace{\begin{Bmatrix} w_1^L \\ w_2^L \\ 2w_3^L - w_3^{L-1} \end{Bmatrix}}_{\text{def } \mathcal{R}} = \underbrace{\begin{Bmatrix} w_1^{L+1,K} \\ w_2^{L+1,K} \\ w_3^{L+1,K} \end{Bmatrix}}_{\text{def } w^{L+1,K}}. \tag{B.5}$$

The eigenvalues of \mathcal{G} are $\lambda^3 = \frac{(\Delta t)^4}{abc}$ and, hence, for convergence we must have

$$|\max \lambda| = \left| \frac{(\Delta t)^4}{abc} \right|^{\frac{1}{3}} < 1. \tag{B.6}$$

One sees that the spectral radius of the staggering operator grows quasilinearly with the time-step size, specifically, super-linearly as $(\Delta t)^{\frac{4}{3}}$.

Generally speaking, if the recursive process is *not employed* (an explicit scheme), the staggering error can accumulate relatively rapidly. *However, an overkill approach involving very small time-steps, smaller than needed to control the discretization error, simply to suppress a non-recursive staggering process error, is computationally inefficient.* Therefore, the objective of the next section is to develop a strategy to adaptively adjust, in fact maximize, the choice of the time-step size to control the staggering error, while simultaneously staying below a critical time-step size needed to control the discretization error. An important related issue is to simultaneously minimize the computational effort involved. The number of times the

²⁰ A Gauss–Seidel-type approach would involve using the most current iterate. Typically, under very general conditions, if the Jacobi method converges, the Gauss–Seidel method converges at a faster rate, while if the Jacobi method diverges, the Gauss–Seidel method diverges at a faster rate. For example, see Ames [3] for details. The Jacobi method is easier to address theoretically, thus it is used for proof of convergence, and the Gauss–Seidel method at the implementation level.

multifield system is solved, as opposed to time-steps, is taken as the measure of computational effort, since within a time-step, many multifield system re-solves can take place.

The result in Eq. (B.6) provides a rough guide for the selection of the exponent (p) for the overall system (when many different types of equations are present). The exponent p is approximately the sum of the product of each field equation that contains a numerical time derivative and the order of the corresponding time differentiation (first order, second order, etc.), divided by the sum of the number of equations using numerical time derivative in the system. Explicitly,

$$p \approx \frac{\sum_{i=1}^N O_i}{N}, \quad (\text{B.7})$$

where N is number of field equations where a numerical derivative was used, and O_i is the order of the time differentiation (first order, second order, etc.) of the individual field equation i . Clearly, p has the following range, $1 \leq p \leq 2$, for a collection of first and second order equations.

References

- [1] A.M. Ahmed, S.E. Elghobashi, Direct numerical simulation of particle dispersion in homogeneous turbulent shear flows, *Phys. Fluids* 13 (2001) 3346–3364.
- [2] A.M. Ahmed, S.E. Elghobashi, On the mechanisms of modifying the structure of turbulent homogeneous shear flows by dispersed particles, *Phys. Fluids* 12 (2000) 2906–2930.
- [3] W.F. Ames, *Numerical Methods for Partial Differential Equations*, second ed., Academic Press, 1977.
- [4] J. Bale-Glickman, K. Selby, D. Saloner, O. Savas, Physiological flow studies in exact-replica atherosclerotic carotid bifurcation, in: *Proceedings of IMECE'03, 2003 ASME International Mechanical Engineering Congress and Exposition*, Washington, DC, 2003, pp. 16–21.
- [5] J. Bale-Glickman, K. Selby, D. Saloner, O. Savas, Experimental flow studies in exact-replica phantoms of atherosclerotic carotid bifurcations under steady input conditions, *J. Biomech. Engrg.* 125 (2003) 38–48.
- [6] P. Barge, J. Sommeria, Did planet formation begin inside persistent gaseous vortices? *A&A* (1995) L1–L4.
- [7] J. Barranco, P. Marcus, O. Umurhan, Scaling & asymptotics of coherent vortices in protoplanetary disks, in: *Proceedings of the 2000 Summer Program – Center for Turbulence Research*, Stanford University Press, 2001, pp. 85–96.
- [8] J. Barranco, P. Marcus, Vortices in protoplanetary disks & the formation of planetesimals, in: *Proceedings of the 2000 Summer Program – Center for Turbulence Research*, Stanford University Press, 2001, pp. 97–108.
- [9] J. Barranco, P. Marcus, Three-dimensional vortices in stratified protoplanetary disks, *Astrophys. J.* 623 (2005) 1157–1170.
- [10] P. Brown, B. Cooke, Model predictions for the 2001 Leonids and implications for Earth-orbiting satellites, *Monthly Notices Royal Astronom. Soc.* 326 (2001) L19–L22.
- [11] S. Beckwith, T. Henning, Y. Nakagawa, Dust particles in protoplanetary disks, in: V. Mannings, A.P. Boss, S.S. Russell (Eds.), *Protostars & Planets IVs*, University of Arizona Press, Tucson, 2000.
- [12] W. Benz, From dust to planets, *Spatium* 6 (2000) 3–14.
- [13] W. Benz, Impact simulations with fracture. 1. Method & tests, *Icarus* 107 (1994) 98–116.
- [14] S.A. Berger, L.D. Jou, Flow in stenotic vessels, *Ann. Rev. Fluid Mech.* 32 (2000) 347–382.
- [15] L. Berlyand, A. Panchenko, Strong and weak blow up of the viscous dissipation rates for concentrated suspensions, *J. Fluid Mech.*, in press.
- [16] L. Berlyand, A. Panchenko, Network approximation for effective viscosity of concentrated suspensions with complex geometries, *SIAM J. Math. Anal.* 36 (5) (2005) 1580–1628.
- [17] J. Blum, G. Wurm, Impact simulations on sticking, restructuring, & fragmentation of preplanetary dust aggregates, *Icarus* 143 (2000) 138–146.
- [18] C. Bohren, D. Huffman, *Absorption and Scattering of Light by Small Particles*, Wiley Science Paperback Series, 1998.
- [19] H. Cho, J.R. Barber, Stability of the three-dimensional Coloumb friction law, *Proc. Royal Soc.* 455 (1983) (1999) 839–862.
- [20] A. Chokshi, A.G.G.M. Tielens, D. Hollenbach, Dust coagulation, *Astrophys. J.* 407 (1993) 806–819.
- [21] C.Y. Chow, *An Introduction to Computational Fluid Dynamics*, Wiley, New York, 1980.
- [22] K.Y. Chyu, P.K. Shah, The role of inflammation in plaque disruption and thrombosis, *Rev. Cardiovas. Med.* 2 (2001) 82–91.
- [23] C.N. Cuzzi, A.R. Dobrovolskis, J.M. Champney, Particle-gas dynamics in the midplane of a protoplanetary nebula, *Icarus* 106 (1993) 102–134.
- [24] M.J. Davies, P.D. Richardson, N. Woolf, D.R. Katz, J. Mann, Risk of thrombosis in human atherosclerotic plaques: role of extracellular lipid, macrophage, and smooth muscle cell content, *Br. Heart J.* 69 (1993) 377–381.
- [25] C. Dominik, A.G.G.M. Tielens, The physics of dust coagulation & the structure of dust aggregates in space, *Astrophys. J.* 480 (1997) 647–673.
- [26] I. St. Doltsinis, Coupled field problems-solution techniques for sequential & parallel processing, in: M. Papadrakakis (Ed.), *Solving Large-scale Problems in Mechanics*, 1993.
- [27] I. St. Doltsinis, Solution of coupled systems by distinct operators, *Engrg. Comput.* 14 (1997) 829–868.
- [28] A. Donev, I. Cisse, D. Sachs, E.A. Varniano, F. Stillinger, R. Connelly, S. Torquato, P. Chaikin, Improving the density of jammed disordered packings using ellipsoids, *Science* 303 (2004) 990–993.
- [29] A. Donev, S. Torquato, F. Stillinger, Neighbor list collision-driven molecular dynamics simulation for nonspherical hard particles-I. Algorithmic details, *J. Comput. Phys.* 202 (2005) 737.
- [30] A. Donev, S. Torquato, F. Stillinger, Neighbor list collision-driven molecular dynamics simulation for nonspherical hard particles-II. Application to ellipses and ellipsoids, *J. Comput. Phys.* 202 (2005) 765.
- [31] O.A. Druzhinin, S.E. Elghobashi, Direct numerical simulation of a three-dimensional spatially-developing bubble-laden mixing layer with two-way coupling, *J. Fluid Mech.* 429 (2001) 23–61.
- [32] C. Farhat, M. Lesoinne, N. Maman, Mixed explicit/implicit time integration of coupled aeroelastic problems: three-field formulation, geometric conservation and distributed solution, *Int. J. Numer. Methods Fluids* 21 (1995) 807–835.
- [33] C. Farhat, M. Lesoinne, Two efficient staggered procedures for the serial and parallel solution of three-dimensional nonlinear transient aeroelastic problems, *Comput. Methods Appl. Mech. Engrg.* 182 (2000) 499–516.

- [34] C. Farhat, G. van der Zee, P. Geuzaine, Provably second-order time-accurate loosely-coupled solution algorithms for transient nonlinear computational aeroelasticity, *Comput. Methods Appl. Mech. Engrg.* 195 (2006) 1973–2001.
- [35] A. Ferrante, S.E. Elghobashi, On the physical mechanisms of two-way coupling in particle-laden isotropic turbulence, *Phys. Fluids* 15 (2003) 315–329.
- [36] M. Frenklach, C.S. Carmer, Molecular dynamics using combined quantum & empirical forces: application to surface reactions, *Adv. Classical Trajectory Methods* 4 (1999) 27–63.
- [37] V. Fuster, *Assessing and Modifying the Vulnerable Atherosclerotic Plaque*, Futura Publishing Company, 2002.
- [38] W. Goldsmith, *Impact: The Theory & Physical Behavior of Colliding Solids*, Dover Re-issue, Toronto, 2001.
- [39] K.R. Grazier, W.I. Newman, W.M. Kaula, J.M. Hyman, Dynamical evolution of planetesimals in the outer solar system I. The Jupiter/Saturn zone, *Icarus* 140 (2) (2000) 341–352.
- [40] K.R. Grazier, W.I. Newman, F. Varadi, W.M. Kaula, J.M. Hyman, Dynamical evolution of planetesimals in the outer solar system II. The Saturn/Uranus & Uranus/Neptune zones, *Icarus* 140 (2) (1999) 353–368.
- [41] J.M. Haile, *Molecular Dynamics Simulations: Elementary Methods*, Wiley, 1992.
- [42] J. Hale, H. Kocak, *Dynamics & Bifurcations*, Springer-Verlag, 1991.
- [43] W.L. Hase, *Molecular Dynamics of Clusters, Surfaces, Liquids, & Interfaces* *Advances in Classical Trajectory Methods*, vol. 4, JAI Press, 1999.
- [44] K. Johnson, *Contact Mechanics*, Cambridge University Press, 1985.
- [45] L.D. Jou, S.A. Berger, Numerical simulation of the flow in the carotid bifurcation, *Theor. Comput. Fluid Mech.* 10 (1998) 239–248.
- [46] A. Kansaal, S. Torquato, F. Stillinger, Diversity of order and densities in jammed hard-particle packings, *Phys. Rev. E* 66 (2002) 041109.
- [47] N. Kikuchi, J.T. Oden, *Contact Problems in Elasticity: A Study of Variational Inequalities & Finite Element Methods*, SIAM, Philadelphia, PA, 1988.
- [48] A. Klarbring, Examples of nonuniqueness & nonexistence of solutions to quasistatic contact problems with friction, *Ingenieur-Archiv.* 60 (1990) 529–541.
- [49] E. Kokubo, S. Ida, Formation of protoplanets from planetesimals in the solar nebula, *Icarus* 143 (1) (2000) 15–270.
- [50] E. Kokubo, S. Ida, On runaway growth of planetesimals, *Icarus* 123 (1) (1996) 180–191.
- [51] M. Lesoinne, C. Farhat, Free staggered algorithm for nonlinear transient aeroelastic problems, *AIAA J.* 36 (9) (1998) 1754–1756.
- [52] P. Le Tallec, J. Mouro, Fluid structure interaction with large structural displacements, *Comput. Methods Appl. Mech. Engrg.* 190 (24-25) (2001) 3039–3067.
- [53] R.W. Lewis, B.A. Schrefler, *The Finite Element Method in the Static & Dynamic Deformation & Consolidation of Porous Media*, second ed., Wiley Press, 1998.
- [54] R.W. Lewis, B.A. Schrefler, L. Simoni, Coupling versus uncoupling in soil consolidation, *Int. J. Numer. Anal. Methods Geomech.* 15 (1992) 533–548.
- [55] P. Libby, Current concepts of the pathogenesis of the acute coronary syndromes, *Circulation* 104 (2001) 365–372.
- [56] P. Libby, The vascular biology of atherosclerosis, in: E. Braunwald, D.P. Zipes, P. Libby (Eds.), *Heart Disease. A Textbook of Cardiovascular Medicine*, sixth, W.B. Saunders Company, Philadelphia, 2001, pp. 995–1009, Chapter 30.
- [57] P. Libby, P.M. Ridker, A. Maseri, Inflammation and Atherosclerosis, *Circulation* 105 (2002) 1135–1143.
- [58] P. Libby, M. Aikawa, Stabilization of atherosclerotic plaques: new mechanisms and clinical targets, *Nat. Med.* 8 (2002) 1257–1262.
- [59] J.J. Lissauer, Planet formation, *ARAA* 31 (1993) 129–174.
- [60] H.M. Loree, R.D. Kamm, R.G. Stringfellow, R.T. Lee, Effects of fibrous cap thickness on peak circumferential stress in model atherosclerotic vessels, *Circ. Res.* 71 (1992) 850–858.
- [61] L. Luo, D.A. Dornfeld, Material removal mechanism in chemical mechanical polishing: theory and modeling, *IEEE Trans.: Semicond. Manufactur.* 14 (2) (2001) 112–133.
- [62] L. Luo, D.A. Dornfeld, Effects of abrasive size distribution in chemical-mechanical planarization: modeling and verification, *IEEE Trans.: Semicond. Manufactur.* 16 (2003) 469–476.
- [63] L. Luo, D.A. Dornfeld, Material removal regions in chemical mechanical planarization for sub-micron integration for sub-micron integrated circuit fabrication: coupling effects of slurry chemicals, abrasive size distribution, and wafer-pad contact area, *IEEE Trans.: Semicond. Manufactur.* 16 (2003) 45–56.
- [64] L. Luo, D.A. Dornfeld, *Integrated Modeling of Chemical Mechanical Planarization of Sub-micron IC Fabrication*, Springer-Verlag, 2004.
- [65] J.A.C. Martins, J.T. Oden, Existence & uniqueness results in dynamics contact problems with nonlinear normal & friction interfaces, *Nonlinear Anal.* 11 (1987) 407–428.
- [66] P. Mitchell, M. Frenklach, Particle Aggregation with Simultaneous Surface Growth, *Phys. Rev. E* 67 (2003) 061407.
- [67] E.A. Moelwyn-Hughes, *Physical Chemistry*, Pergamon, 1961.
- [68] J.T. Oden, E. Pires, Nonlocal & nonlinear friction laws & variational principles for contact problems in elasticity, *ASME J. Appl. Mech.* 50 (1983) 67–76.
- [69] J.N. Pollack, D. Hollenbach, S. Beckwith, D.P. Simonelli, T. Roush, W. Fong, Composition & radiative properties in molecular clouds & accretion disks, *Astrophys. J.* 421 (1994) 615–639.
- [70] K.C. Park, C.A. Felippa, Partitioned analysis of coupled systems, in: T. Belytschko, T.J.R. Hughes (Eds.), *Computational Methods for Transient Analysis*, 1983.
- [71] S. Piperno, Explicit/implicit fluid/structure staggered procedures with a structural predictor & fluid subcycling for 2D inviscid aeroelastic simulations, *Int. J. Numer. Meth. Fluids* 25 (1997) 1207–1226.
- [72] S. Piperno, C. Farhat, B. Larrouturou, Partitioned procedures for the transient solution of coupled aeroelastic problems – Part I: Model problem, theory, and two-dimensional application, *Comput. Methods Appl. Mech. Engrg.* 124 (1-2) (1995) 79–112.
- [73] S. Piperno, C. Farhat, Partitioned procedures for the transient solution of coupled aeroelastic problems – Part II: Energy transfer analysis and three-dimensional applications, *Comput. Methods Appl. Mech. Engrg.* 190 (2001) 3147–3170.
- [74] D.C. Rapaport, *The Art of Molecular Dynamics Simulation*, Cambridge University Press, 1995.
- [75] P.D. Richardson, M.J. Davies, G.V.R. Born, Influence of plaque configuration and stress distribution on fissuring of coronary atherosclerotic plaques, *Lancet* 2 (8669) (1989) 941–944.
- [76] T. Schlick, *Molecular Modeling & Simulation An Interdisciplinary Guide*, Springer-Verlag, New York, 2000.
- [77] L. Schmidt, *The Engineering of Chemical Reactions*, Oxford University Press, 1998.

- [78] B.A. Schrefler, A partitioned solution procedure for geothermal reservoir analysis, *Comm. Appl. Num. Meth.* 1 (1985) 53–56.
- [79] P.K. Shah, Plaque disruption and coronary thrombosis: new insight into pathogenesis and prevention, *Clinical Cardiol.* 20 (suppl. II) (1997) II-38–II-44.
- [80] F.H. Stillinger, T.A. Weber, Computer simulation of local order in condensed phases of silicon, *Phys. Rev. B* 31 (1985) 5262–5271.
- [81] J.S. Stroud, S.A. Berger, D. Saloner, Numerical analysis of flow through a severely stenotic carotid artery bifurcation, *J. Biomed. Engrg.* 124 (1) (2002) 9–21.
- [82] J.S. Stroud, S.A. Berger, D. Saloner, Influence of stenosis morphology on flow through severely stenotic vessels: implications of plaque rupture, *J. Biomech.* 33 (2000) 443–455.
- [83] K.D. Supulver, D.N.C. Lin, Formation of icy planetesimals in a turbulent solar nebula, *Icarus* 146 (2) (2000) 525–540.
- [84] P. Tanga, A. Babiano, B. Dubrulle, A. Provenzale, Forming planetesimals in vortices, *Icarus* 121 (1) (1996) 158–170.
- [85] S. Torquato, *Random Heterogeneous Materials: Microstructure and Macroscopic Properties*, Springer-Verlag, New York, 2002.
- [86] J. Tersoff, Empirical interatomic potential for carbon, with applications to amorphous carbon, *Phys. Rev. Lett.* 61 (1988) 2879–2882.
- [87] A.C. van der Wal, A.E. Becker, Atherosclerotic plaque rupture – pathologic basis of plaque stability and instability, *Cardiovasc. Res.* 41 (1999) 334–344.
- [88] S.J. Weidenschilling, J.N. Cuzzi, Formation of planetesimals in the solar nebula, in: E.H. Levy, J.I. Lunine (Eds.), *Protostars & Planets III*, University of Arizona Press, Tucson, 1993, pp. 1031–1060.
- [89] S.J. Weidenschilling, D. Spaute, D.R. Davis, F. Marzari, K. Ohtsuki, Accretional evolution of a planetesimal swarm, *Icarus* 128 (2) (1997) 429–455.
- [90] B. Widom, Random sequential addition of hard spheres to a volume, *J. Chem. Phys.* 44 (1966) 3888–3894.
- [91] P. Wriggers, *Computational Contact Mechanics*, John-Wiley, 2002.
- [92] G. Wurm, J. Blum, J.E. Colwell, A new mechanism relevant to the formation of planetesimals in the solar nebula, *Icarus* 151 (2001) 318–321.
- [93] O.C. Zienkiewicz, Coupled problems & their numerical solution, in: R.W. Lewis, P. Bettes, E. Hinton (Eds.), *Numerical Methods in Coupled Systems*, Wiley, Chichester, 1984, pp. 35–58.
- [94] T.I. Zohdi, An adaptive-recursive staggering strategy for simulating multifield coupled processes in microheterogeneous solids, *Int. J. Numer. Methods Engrg.* 53 (2002) 1511–1532.
- [95] T.I. Zohdi, Modeling and simulation of a class of coupled thermo-chemo-mechanical processes in multiphase solids, *Comput. Methods Appl. Mech. Engrg.* 193 (6–8) (2004) 679–699.
- [96] T.I. Zohdi, Modeling and direct simulation of near-field granular flows, *Int. J. Solids Struct.* 42/2 (2004) 539–564.
- [97] T.I. Zohdi, A computational framework for agglomeration in thermo-chemically reacting granular flows, *Proc. Royal Soc.* 460 (2052) (2004) 3421–3445.
- [98] T.I. Zohdi, Charge-induced clustering in multifield granular flow, *Int. J. Numer. Methods Engrg.* 62 (7) (2005) 870–898.
- [99] T.I. Zohdi, G.A. Holzapfel, S.A. Berger, A phenomenological model for atherosclerotic plaque growth and rupture, *J. Theor. Biol.* 227 (3) (2004) 437–443.
- [100] T.I. Zohdi, A simple model for shear stress mediated lumen reduction in blood vessels, *Biomech. Model. Mechanobiol.* 4 (1) (2005) 57–61.